POWER SYSTEM ANALYSIS AND OPTIMIZATION FOR BIOAPPS ROMICP® FOOT PROSTHESIS

MOHAMMAD BILAL GOOLFEE

FACULTY OF ENGINEERING
UNIVERSITY OF MALAYA
KUALA LUMPUR

2021

POWER SYSTEM ANALYSIS AND OPTIMIZATION FOR BIOAPPS ROMICP® FOOT PROSTHESIS

MOHAMMAD BILAL GOOLFEE

THESIS SUBMITTED IN PARTIAL FULFILMENT OF THE REQUIREMENTS FOR THE DEGREE OF MASTER OF BIOMEDICAL ENGINEERING

FACULTY OF ENGINEERING
UNIVERSITY OF MALAYA
KUALA LUMPUR

2021

UNIVERSITY OF MALAYA

ORIGINAL LITERARY WORK DECLARATION

Name of Candidate: Mohammad Bilal Goolfee

Matric No: S2008718

Name of Degree: Master of Biomedical Engineering

Title of Project Paper/Research Report/Dissertation/Thesis ("this Work"):

Power System Analysis And Optimization For BioApps RoMicP® Foot Prosthesis

Field of Study: Biomechanics, Power Electronics

I do solemnly and sincerely declare that:

(1) I am the sole author/writer of this Work;
(2) This Work is original;
(3) Any use of any work in which copyright exists was done by way of fair dealing and for permitted purposes and any excerpt or extract from, or reference to or reproduction of any copyright work has been disclosed expressly and sufficiently and the title of the Work and its authorship have been acknowledged in this Work;
(4) I do not have any actual knowledge nor do I ought reasonably to know that the making of this work constitutes an infringement of any copyright work;
(5) I hereby assign all and every rights in the copyright to this Work to the University of Malaya ("UM"), who henceforth shall be owner of the copyright in this Work and that any reproduction or use in any form or by any means whatsoever is prohibited without the written consent of UM having been first had and obtained;
(6) I am fully aware that if in the course of making this Work I have infringed any copyright whether intentionally or otherwise, I may be subject to legal action or any other action as may be determined by UM.

Candidate's Signature Date:

Subscribed and solemnly declared before,

Witness's Signature Date:

Name:

Designation:

POWER SYSTEM ANALYSIS AND OPTIMIZATION FOR BIOAPPS ROMICP® FOOT PROSTHESIS

ABSTRACT

A critical component of a motor-powered prosthesis is the power system that generates the required torque at the joint by converting chemical energy stored in batteries into electrical energy and finally mechanical torque. Prior studies focus mainly on the control system of prostheses and barely cover the power component. In order to achieve high power efficiency in the RoMicP® prosthesis, this study investigates the required battery specifications through calculations, as well as the power consumption of the LMG5200 inverter system and the feasibility of a multilevel inverter configuration using the simulation model and software (available online) from the manufacturer, Texas Instrument. The results showed that to fulfil the design requirement of weighing below 2.5kg, the battery size required is 10Ah at 24V and can power the prosthesis for 5k steps per day. Moreover, using the LMG5200, an efficiency of 99.72% was achieved through PWM switching with harmonic distortion of 2.15% for a three-phase output. Furthermore, the proposed multi-level inverter design achieved an efficiency of 59.46% with harmonic distortion of 0.82% and could therefore not be recommended for use in this case, although it demonstrated that a multi-level system could generate cleaner output. In summary, this project successfully investigated the battery requirements, power consumption and efficiency of the simulated system, as well as the feasibility of a multi-level inverter topology. Future studies should focus on investigating other multi-level topologies, and increasing the number of levels, as well as different advanced switching techniques such as Space Vector Modulation.

Keywords: Biomechanics, power electronics, prosthesis, inverter, multi-level inverter.

ACKNOWLEDGEMENTS

All praise be to The Almighty for His favors and the opportunity to successfully complete this work and the Master studies despite the difficult situation with COVID-19.

I extend my most sincere gratitude to Prof. Ir. Dr. Noor Azuan Abu Osman for his tireless support, advice, guidance and help throughout the course of this work and beyond. His contribution to this work has been a major pillar in its success.

I would also like to thank Mr Mouaz Al Kouzbary for taking the time to discuss this work and his help and assistance to achieve the goals set out for this work.

Thanks also go to my family, without whom this work would not have been achieved, for their support and help throughout my studies. A special thought to my late grandmother, whose terminal health condition motivated me to pursue more knowledge in the field of Biomedical Engineering to contribute to the betterment of human health.

Finally, I would like to thank my colleagues and friends for the experience we shared throughout the course of this study.

TABLE OF CONTENTS

LIST OF FIGURES

LIST OF TABLES

LIST OF SYMBOLS AND ABBREVIATIONS

AC	:	Alternating current
BLDC	:	Brushless direct current motor
DC	:	Direct current
FET	:	Field-effect transistor
GaN	:	Gallium-nitride
IGBT	:	Insulated-gate bipolar transistor
MLI	:	Multilevel inverter
MOSFET	:	Metal-oxide-semiconductor field-effect transistor
PMSM	:	Permanent magnet synchronous motor
PWM	:	Pulse-width modulation
RLC	:	Resistor, inductor, capacitor
RMS	:	Root mean square
TI	:	Texas Instruments

LIST OF APPENDICES

CHAPTER 1: INTRODUCTION TO THE STUDY

1.1 Introduction

Every year, approximately 60,000 patients undergo a lower extremity amputation in the United States (Bernatchez, Mayo, & Kayssi, 2021). It is estimated that by 2050 the total number of amputees in the United States alone will rise to 3.6 million, double the current number (Ziegler-Graham, MacKenzie, Ephraim, Travison, & Brookmeyer, 2008). These numbers show an alarming need for better lower limb prosthetics that can provide an almost natural response, since the amount of energy expensed by an amputee is up to 120% higher than a normal person (Su, Gard, Lipschutz, & Kuiken, 2007). A study by Jarvis et al. (2017) showed that the gait pattern of amputees can be greatly improved by means of proper prosthetics, bringing the energy expensed to a comparable level to normal gait.

Over the course of the last 20 years, significant progress has been achieved in the area of leg prosthetics, including foot, ankle and knee as pointed out by Tucker et al. (2015). Liu et al. (2021) showed in their analysis that most ankle-foot prostheses could be classified as either purely mechanical, hydraulic or pneumatic-based, or motorized. Their research, as well as previous ones such as Jarvis et al. (2017), also point to the advantages of motorized systems over the others mainly due to natural gait-cycle mimicking, and since the former is less complicated compared to pneumatic or hydraulic systems which are bulkier and more inconvenient.

The system under investigation in this project is the BioApps RoMicP® Foot-Ankle Prosthesis developed by Al Kouzbary, Abu Osman, Al Kouzbary, Shasmin, and Arifin (2020). While the mechanical specifications and the control systems of the prosthesis have been studied, there is still one area that needs further investigation and understanding, and that is the power system. Biomechatronic prostheses combine the fields of mechanics, electronics, and biology to create prosthetic solutions, and while there are extensive research in the area of biomechanics, research into electronic integration is still limited (Lechler et al., 2018).

This project will therefore study and analyze the power system of the BioApps RoMicP® Foot-Ankle Prosthesis in order to optimize the system and determine the proper battery technology required to fulfill the design requirements of the prosthesis.

1.2 Research Problem

Research done by Hobusch, Döring, Brånemark, and Windhager (2020) showed that data regarding gait patterns and kinematics for powered lower limb prostheses is scarce. Further investigation also showed that data regarding the electrical and electronic components applied in the field of biomechatronic and robotic prosthetics is virtually non-existent.

Therefore, the first challenge that has to be investigated is the application of power electronics in prosthesis design. A computer model of the power electronic system (inverter system) has to be designed in order to understand and analyze its performance through simulations.

Furthermore, the system needs to be adaptable to different configurations of electrical or electronic components that will enable further development and optimization of the prosthesis.

1.3 Research Objectives

In order to overcome the challenges faced with the BioApps RoMicP® Foot Prosthesis, this project aims to analyze and optimize the power system of the prosthesis through the following objectives:

- To investigate suitable battery specifications to fulfil the design criteria of the ankle-foot prosthesis.
- To study the power consumption and efficiency of the simulated inverter system.
- To evaluate the feasibility of using a multi-level 3-phase inverter and its impact on power consumption.

1.4 Organization of Report

The upcoming chapters of this report are arranged in the following order: Chapter 2 covers the literature review of research in the areas of ankle-foot prostheses, single- and multi-level 3-phase motor inverters, and battery technologies employed in similar devices.

In Chapter 3, the research design and methodology to be used to carry out this project are discussed, covering the different parameters to be considered, what parameters to measure and how to achieve satisfactory results.

Chapter 4 presents the results obtained through the data from various tests conducted and an analysis of these results to fulfil the objectives previously defined.

Chapter 5 provides a discussion of the results obtained and possible sources of errors and possible improvements to be explored.

Finally, Chapter 6 highlights the key points of this research as well as providing recommendations for future implementations, thus concluding this project.

CHAPTER 2: LITERATURE REVIEW

In this chapter, previous work in the area of high-power inverters for robotic prosthesis will be reviewed for a deeper understanding of the current state of ankle-foot prostheses, i.e., the challenges faced, and possible ways of overcoming them.

In a recent study, Liu et al. (2021) compared 91 powered prostheses and categorized motor-driven ones into nine classes. The authors also reported the scarcity of commercialized motor-powered prostheses owing to various uncertainties, despite the advantages of motorized prostheses. Refer to Liu et al. (2021) for full comparison between different powered prostheses.

2.1 Electrical Motors

Motorized foot prosthetics have come a long way to assist amputees in performing daily tasks without many restrictions. With these advancements, there are now more opportunities to enhance such systems from different angles. One important component of modern prosthetics is the motor being used. In this section, previous work related to motors and inverters will be reviewed.

There is usually a preference for *alternating current* (AC) motors compared to *direct current* (DC) motors since the latter is less efficient and requires more maintenance: the brushes and commutators have to frequently be replaced to maintain optimum operating conditions (Mahesh, Angadi, & Raju, 2018). Moreover, for the same power ratings, the size of a DC motor is larger than that of an AC motor, while the price of the former is twice as much as that of the latter (Mahesh et al., 2018). As such, this review will focus on works that make use of AC motors.

The most common type of AC motor is the three-phase induction motor which comprises of 2 major components: the stator and the rotor (Hughes, 2006). The stator is the stationary part of the motor which houses 3 separate coil windings, each connected to one phase of the AC supply. As the AC passes through the windings, a changing (rotating) magnetic field is generated due to the change in amplitude of the supply. This induces a current in the rotor, located within the stator, which generates its own magnetic field. The rotor starts to rotate as its magnetic field is repelled by that of the stator. The speed of rotation is controlled by the frequency of the AC current.

Ershad and Mehrjardi (2018) in their study discussed the numerous advantages of three-phase motors over single-phase ones. Among the advantages are the lower cost of three-phase motors due to their simpler construction, smaller physical sizes, higher efficiency, and lower starting current. These make 3-phase motors ideal for applications where size and efficiency are major considerations.

Two common types of motors include: permanent magnet synchronous motor (PMSM) and brushless DC motor (BLDC), and they are both inexpensive and widely used (Sakunthala, Kiranmayi, & Mandadi, 2017). In their comparison of these 2 types of motors, Sakunthala et al. (2017) highlighted the similarities between both motors and since both use permanent magnets, they have high efficiency, are easy to control, and can produce high torque. The major difference between the 2 lies in the back electromotive force (EMF) produced: PMSM produces a sinusoidal back EMF while BLDC produces a trapezoidal back EMF.

In a study to compare different types of motors, Derammelaere, Haemers, Viaene, Verbelen, and Stockman (2016) commented on the suitability of each motor type for varying applications: high speed applications suit BLDC motors, while PMSM are better suited for high torque and have higher power density, thus have better performance. The authors also highlighted that the main difference in the construction of each motor is in the location of permanent magnets in each type of motor: BLDC has permanent magnets in the rotor while in PMSM they are located in the stator.

To summarize, while there exist numerous types of motors, AC motors are preferred over DC motors because of efficiency and relative size for the desired application. A comparison between the reviewed types of electrical motors is given in Table 2.1 below.

Table 2.1: Review of electric motors

Authors	Motor Type	Properties
(Mahesh et al., 2018)	DC	Larger Size, More expensive
	AC	More efficient, less maintenance
(Ershad & Mehrjardi, 2018)	3-Phase	Lower cost, small size, high efficiency, low starting current
(Sakunthala et al., 2017)	PMSM	Inexpensive, high efficiency, high torque
	BLDC	Inexpensive, high efficiency, high torque
(Derammelaere et al., 2016)	PMSM	High torque application, better performance
	BLDC	High speed application, low power density

Based on the summary shown in Table 2.1, the most suitable type of motor to be used for the RoMicP® prosthesis is the PMSM 3-phase AC motor due to its low price, high efficiency, high torque, and better performance compared to other types of motors.

2.2 Battery Technologies

To power the motors used in prosthetics, batteries are required to allow freedom of movement to the patient. While batteries have been accessible and extensively used in numerous fields, documentation in relation to motorized prosthetics is limited. Hence, in this section, some of the numerous battery technologies currently being used will be explored.

In their experiment to automatically map the forces applied by an amputee on a mock prosthesis, Rossi, Rizzi, Lorenzelli, and Brunelli (2016) designed a battery-powered sensor system in which they make use of a lithium-ion battery pack rated at 7.5V with a capacity of 2.2Ah, which powered a 750mW system for up to 8 hours. Their supply system used a linear regulator at 5V to power the sensors, amplifiers, and multiplexer circuits while the rest of the circuit was powered by a linear regulator at 3.1V. The main benefit highlighted by the authors was in the long battery life even while the system is constantly communicating through Wi-Fi.

Hu, You, Chen, McCormick, and Budgett (2016) proposed a wireless power supply for brain implant devices in which they make use of a lithium-ion battery with a power rating of 3.7V with a capacity of 70mAh. With a constant power draw of 32mW, the battery was operational for approximately 75 minutes. The authors highlighted the dangers of lithium-ion batteries including catching fire or explosions if not handled properly. They also noted the rapid lifecycle reduction if the batteries are overcharged or discharged and to mitigate this issue, Hu et al. (2016) made use of a linear-mode lithium-ion charging circuit (BQ2057C).

To compensate for body temperature fluctuations between 37 to 40 degrees in implantable devices, Lee, Dai, and Chuang (2018) aimed to accurately estimate the state-of-charge of the battery in their experiment. They concluded from their experiment that the error margin of their system was within 3%. The author used a lithium-ion polymer battery rated at 3.7V with a capacity of 630mAh. Their physical experiment determined that the rated capacity of the battery increased to 621.8mAh at 40 degrees from 611.6 at 37 degrees, although both were below the rated capacity.

In an attempt to lower the overall cost of a prosthetic arm, Hussian et al. (2018) made use of a 3.7V battery rated at 2300mAh. However, the authors only measured the charging rate of the battery by making use of piezoelectric generators placed in the shoes of the patient. They concluded, through their experiment, that the average person is able to recharge the battery by making use of 4 piezoelectric generators and 1.3 miles walk, the equivalent of 2750 steps. This may prove to be useful especially when using motorized foot prostheses to recover energy spent while walking.

In a recent study into the fabrication of a rechargeable battery for biomedical devices, Harilal, Ramachandran, Satheesh Babu, and Suneesh (2020) explored the possibility of using silver peroxide-zinc instead of lithium-ion in order to overcome the limitations of the latter. They designed two models of rechargeable batteries, namely a compartment type and a pouch type. The two-compartment prototype was able to deliver 150μW, which resulted in a 1.5-hour operation time with a load of 20mA at 1.5V (0.03W). Although the results seem promising for this new type of battery, it is still in prototyping stage and might not be readily available in the near future.

From the works reviewed with regards to the battery technologies used, it was observed that most experiments made use of lithium-ion polymer batteries. Table 2.2 below summarizes the batteries used in the reviewed works and their relevant parameters.

Table 2.2: Review of battery technologies

Author	Technology	Voltage/ V	Rating/ mAh	Energy/ Wh	Load/ W	Description
(Rossi et al., 2016)	Lithium-ion	7.5	2200	16.5	0.75	8 hours
(Hu et al., 2016)	Lithium-ion	3.7	70	0.259	0.032	75 minutes
(Lee et al., 2018)	Lithium-ion	3.7	630	2.331	-	-

(Hussian et al., 2018)	Piezo-electric generator	3.7	2300	8.51	-	2750 steps to recharge
(Harilal et al., 2020)	Silver peroxide-zinc	7.5	2.6	0.0195	0.03	1.5 hours

From Table 2.2, it can be inferred that Lithium-ion batteries were the most common types of batteries in use and provide ample energy to drive loads for extended hours, provided they have the necessary charge and discharge protection circuits.

2.3 Inverters

Three-phase motors require AC signal to operate while batteries produce DC signals. In order to use a battery to operate a three-phase motor, a device (or circuit) that converts the DC signal into AC is required. One such device that converts DC into a continuous AC signal is known as an inverter (Patin, 2015). In this section, past work related to DC-to-AC inverters will be reviewed.

A typical three-phase inverter consists of 3 half-bridges, shown in Figure 2.1 below, that get switched at specified times to generate alternating signals shifted 120 degrees from one another (Patin, 2015). The switching is commonly achieved using semiconductors, especially field-effect transistors (FET) due to their rapid switching and low power required (Manias, 2017).

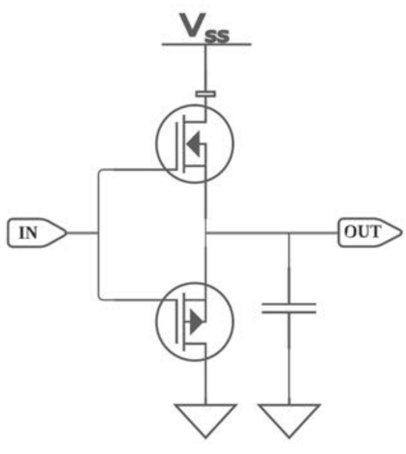

Figure 2.1: A typical single-phase inverter (Rout, Nayak, & Acharya, 2013)

Ismayil kani, Manikandan, and Premkumar (2021) proposed a soft switching inverter controlled by an artificial neural network “to achieve zero voltage switching”. The system was simulated in MATLAB/Simulink and results showed that the proposed system was superior to other systems using fuzzy logic or proportional-integral control. With a DC input of 240V, the simulation produced an output of 120Vrms from a switching frequency of 50kHz.

Comparing the efficiency between silicon carbide (SiC) metal-oxide-semiconductor field-effect transistor (MOSFET) and silicon (Si) insulated-gate bipolar transistors (IGBT) for electric vehicles, Ding, Du, Zhou, Guo, and Zhang (2017) concluded that the MOSFET produced less heat resulting in higher thermal conductivity, as well as higher power density and lower losses. At low speed, the efficiency of the MOSFET was higher than 99% compared to 96% from the IGBT setup. Similar observations were also made by Feng et al. (2014) in comparing Si and SiC MOSFETs.

In a different comparison between conventional Si MOSFETs and gallium-nitride (GaN) MOSFETs carried out by Hasan (2017), the author concluded that the overall performance of GaN-based MOSFET was higher than Si-based MOSFET. The author also highlighted the lower leakage current of GaN MOSFETs, their larger voltage operation range and lower power consumption due to the lower switching voltage required.

In summary, from comparison studies previously carried out on the different types of transistors, GaN-based transistors perform better as inverting switching devices. In order of higher performance to lower, the transistors used can be classified as follows: GaN MOSFET, SiC MOSFET, Si MOSFET, and Si IGBT. Table 2.3 below summarizes the reviewed types of transistors used as inverters and their properties.

Table 2.3: Inverter comparison

Authors	Transistor Type	Properties
(Ding et al., 2017)	Si IGBT	More heat and more losses Lower power density Less efficient (96%)
	SiC MOSFET	Less heat and lower losses Higher power density More efficient (99%)
(Hasan, 2017)	Si MOSFET	Lower performance Higher power consumption Higher switching voltage
	GaN MOSFET	Higher performance Lower power consumption Lower switching voltage

It can be concluded from Table 2.3 above that although different types of transistors can be used as switching devices, the best performance and lowest power consumption can be achieved via GaN-FET, making the latter the best candidate for applications using batteries.

2.4 Multi-Level Inverters

To overcome the limitations of single level inverters, multilevel (three or more levels) ones are used. According to Koshti and Rao (2017), three main types of multilevel inverters (MLI) exist, namely: diode clamped, flying capacitor, and cascaded H-bridge. On one hand, the advantages that MLI provide include: pure sinusoidal waveform, reduced Harmonic effect, reduced switching losses, and less stress on motors among others (Krishna & Suresh, 2016). On the other hand, the main shortcomings of MLI are the high price and complexity due to the higher number of switches needed.

Irrespective of the type of MLI used, the benefits achieved are similar (Jana, Biswas, & Das, 2017). Jana et al. (2017) also highlight that the cascaded inverter eliminates the need for diode clamping or capacitors, as well as making use of less segments compared to the other types, all while maintaining a straightforward control owing to the identical structure.

Using PWM switching, Vijayalakshmi, Hubert Tony Raj, Palaniyappan, and Rajkumar (2020) were able to control the output modulation of a H-bridge cascaded MLI in a review of the latter. Figure 2.2 below shows a generic H-bridge cascaded MLI connected to a 3-phase motor.

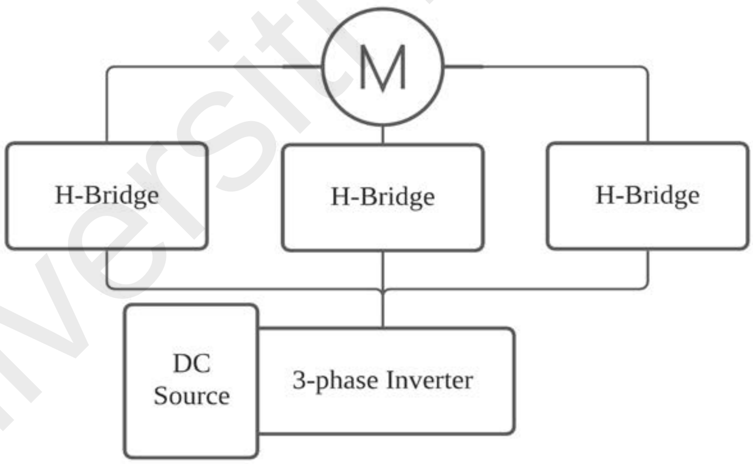

Figure 2.2: Cascaded MLI with 3-phase motor (Vijayalakshmi et al., 2020)

Vijayalakshmi et al. (2020) successfully enhanced the AC signal generated by the MLI, and hence its performance, by employing an inductor-less approach combined with the PWM switching. The system was simulated using PSIM and the schematic model of one of the H-bridges is shown in Figure 2.3 below. Symbols S1 to S4 represent the MOSFET switches used, D1 to D4 represent clamping diodes between the source and drain of each MOSFET, and C represent a capacitor across both half-bridges.

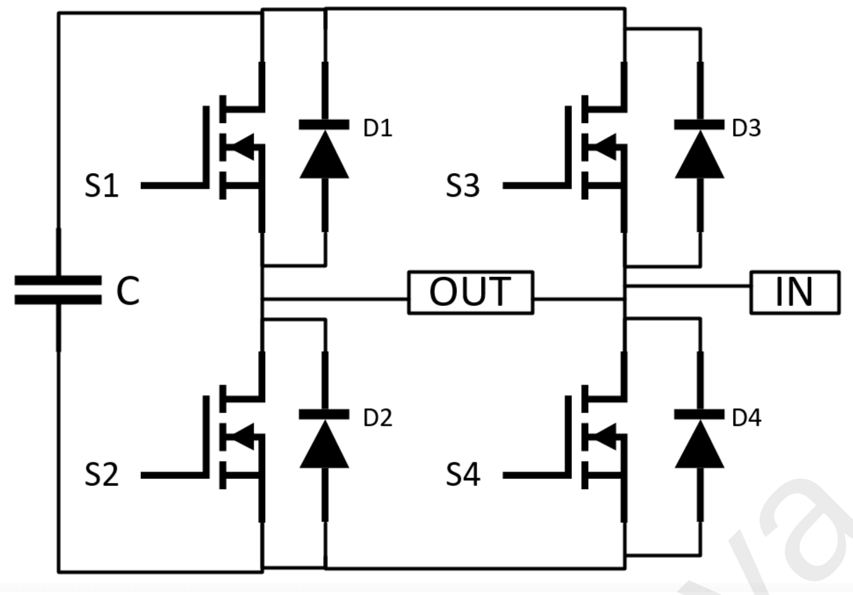

Figure 2.3: PSIM model of H-bridge cascaded MLI(Vijayalakshmi et al., 2020)

Similarly, Maheswari, Bharanikumar, Arjun, Amrish, and Bhuvanesh (2020) highlighted in their review that the H-bridge cascaded MLI is more significant than other types even though the latter are still used in numerous applications. With cascaded MLI, the number of switching devices can be reduced and by applying modified pulse-width modulation (PWM), the output levels are improved.

In a survey by Rodriguez, Jih-Sheng, and Fang Zheng (2002), the major topologies of MLI were discussed along with their control methods and their typical applications. In their discussion of the application in power systems, the authors highlighted that capacitor-clamped inverters are unsuitable for reactive power compensation while the cascaded H-bridge inverter is more suitable for such applications.

The different MLI topologies were conveniently summarized by Venkataramanaiah, Suresh, and Panda (2017) in their review of the former. First, there are symmetrical MLIs where the DC supplies have equal value and the finest system was proposed by Alishah, Nazarpour, Hosseini, and Sabahi (2014) due to the small size, low cost, and lower switch count. Secondly, when the DC input values are not equal at all inputs, the MLI is referred to as asymmetric. Babaei, Alilu, and Laali (2014) proposed a MLI which had the most levels using fewer IGBT. The model with lowest number of IGBTs was proposed by Alishah et al. (2014) and the model with the least number of DC sources was proposed by Babaei, Kangarlu, and Sabahi (2014).

In summary, while there exit different types of MLI, most researchers recommend the use of H-bridge cascaded MLI due to their numerous benefits such as reduced number of switching devices and improved AC signal generation. Table 2.4 below summarizes the reviewed MLI systems and the benefits of each.

Table 2.4: MLI comparison

Author	MLI Type	Benefits
(Jana et al., 2017)	Cascaded	No diodes or capacitors needed, less segments
(Vijayalakshmi et al., 2020)	Cascaded H-bridge with PWM switching	Enhanced AC signal, inductors not required
(Maheswari et al., 2020)	Cascaded H-bridge with PWM switching	Fewer switching devices, output levels improved
(Rodriguez et al., 2002)	Cascaded H-bridge vs capacitor clamped	Cascaded H-bridge better for reactive power compensation

2.5 Simulation of Inverter Circuits

In this section, previous works related to the simulation of inverter systems will be reviewed to provide a deeper understanding of the methods, tools, and applications used, as well as how results were presented in different cases.

In a comparative study between a two-level and five-level inverter system, Jana et al. (2017) employed a MATLAB/Simulink simulation model of their systems to analyze the inverter response in each case. Each system and each phase were simulated separately, and the results finally compared. Their system comprised of a supercapacitor as source, the inverter circuit and a PMSM load. Figure 2.2 below shows the simulation block diagram for one phase of the 3-phase 5-level inverter system. From their experiment, the authors concluded that the outputs of the 5-level inverter were closer to an ideal waveform, with a more regular response from the supercapacitor source.

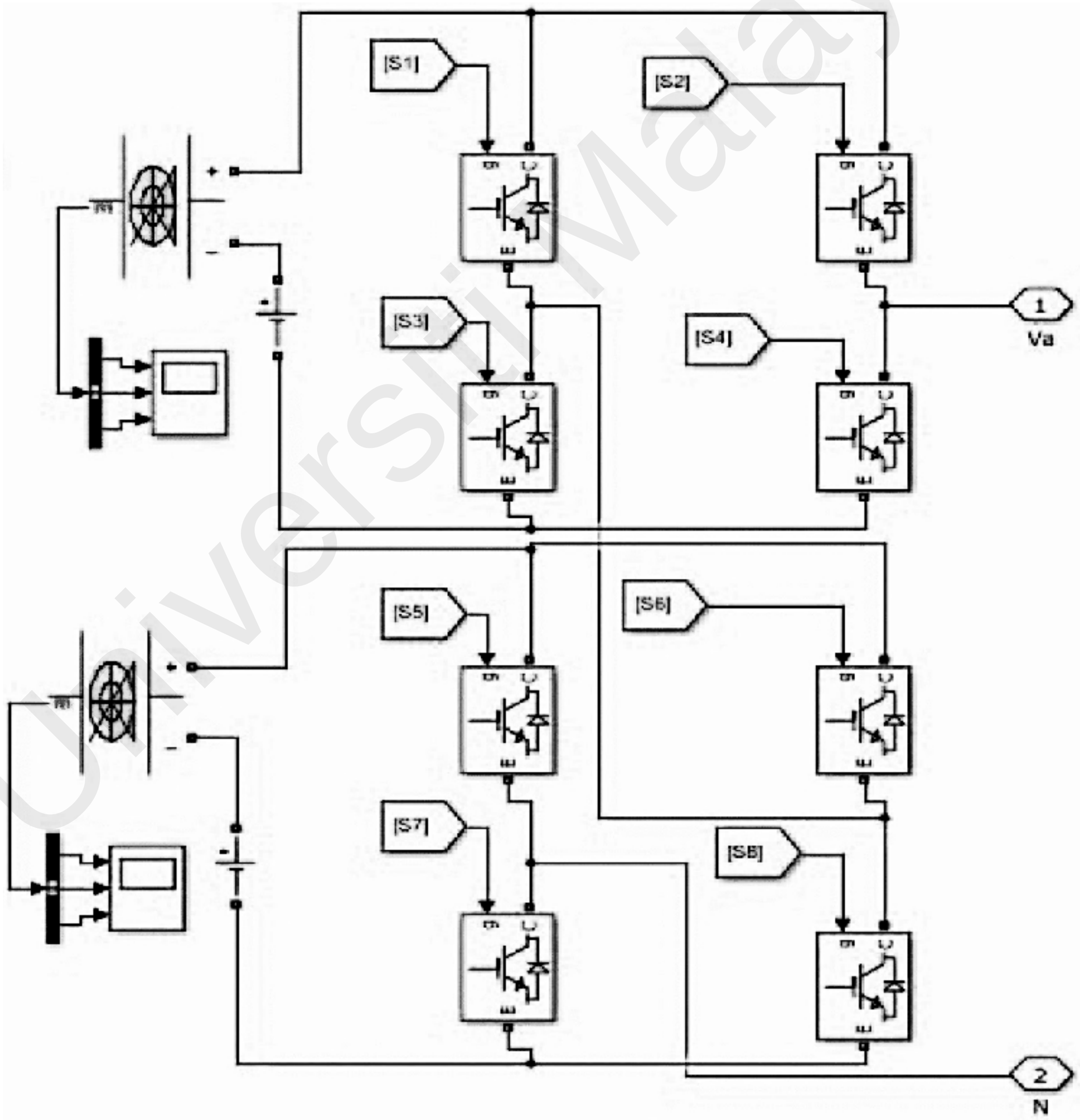

Figure 2.4: Simulation diagram of 3-phase 5-levels inverter(Jana et al., 2017)

In a recent simulation experiment to model a 3-phase MLI, Qanbari and Tousi (2021) combined 2 single-phase H-bridge inverters and a conventional 3-phase inverter. To compensate for the need of multiple sources, transformers are used. Unfortunately, this increases the complexity, and adds extra bulk to the system – a major disadvantage for applications where mobility is key. Using MATLAB and the PSCAD tool, the simulation was carried out and the proposed model was experimentally validated with a power efficiency of 94%.

Thiyagarajan (2020) presented a 51-level inverter simulated in MATLAB/Simulink comprising of 6 DC sources and 12 power electronic switches. To validate the results, the author compared the system to other recent models that were comparable in terms of number of sources and switches.

Table 2.5 below summarizes the different tools used to run the simulations for the different inverter systems and the results obtained in relation to the simulations.

Table 2.5: Simulation Comparison

Author	Inverter System	Simulation Tool	Results
Jana et al. (2017)	Compare 2-level and 5-level inverter	MATLAB/Simulink	5-level waveform closer to ideal
Thiyagarajan (2020)	51-level inverter with 6 DC sources	MATLAB/Simulink	Validated with other recent models
Vijayalakshmi et al. (2020)	3-phase cascaded H-bridge MLI	PSIM	AC signal waveform enhanced
Qanbari and Tousi (2021)	3-phase MLI with transformers	MATLAB and PSCAD	Efficiency of 94%

2.6 Summary

In Chapter 2, a review of past work concerning the different important components involved in the power system of the foot prosthesis has been performed. Antivachis, Niklaus, Bortis, and Kolar (2021) illustrated an accurate representation of the system being analyzed in this project, shown in Figure 2.5 below.

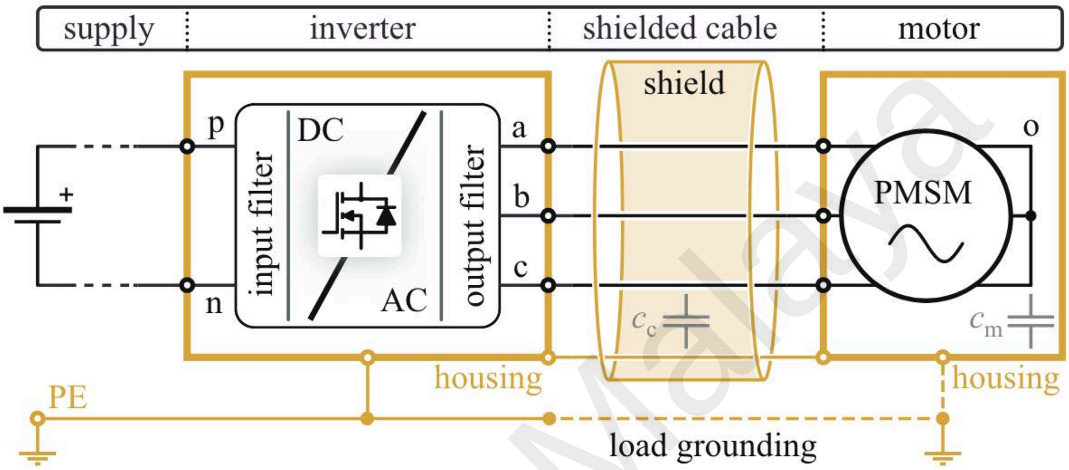

Figure 2.5: Generic power system components (Antivachis et al., 2021)

The system consists of a DC supply, typically a battery that is connected to an inverter system. The inverter system includes input and output filters and FET switches (soft switches) which convert the DC signal into 3-phase AC which is then fed to a PMSM motor by means of a shielded cable.

Chapter 2 also reviewed the different types of motors and batteries being used in the field currently. It was found that the PMSM 3-phase motor provides better performance and the most common type of battery used is the lithium-ion.

Moreover, it was also observed that the most favorable type of inverter is the H-bridge cascaded MLI, which can generate more stable and better performing output AC signal. These results were obtained mainly in MATLAB/Simulink, PSCAD, and/or PSIM simulations of the systems.

CHAPTER 3: METHODOLOGY

3.1 Introduction

In this chapter, the methodology used to achieve the objectives stated in Chapter 1.3 for the RoMicP® foot prosthesis will be discussed.

3.2 Design Constraints

In order to properly design and analyze the battery-powered system, the design criteria of the prosthesis have to be established. The total number of level-ground walking steps can have a value of 5,000 if the total steps include both legs, and if only the amputated leg is considered, the total steps become 10,000. The average weight of a Malaysian male was obtained from data from WorldData.info . Table 3.1 below summarizes the design criteria of the RoMicP® foot prosthesis.

Table 3.1: Design criteria for the RoMicP® foot prosthesis

Criterion	Value
Maximum weight of prosthesis	2.5 kg
Maximum number of steps per day	5,000 or 10,000
Average weight of subjects	71.5 kg

3.3 Battery Selection

To proceed with selecting the correct battery technology with the correct parameters, the overall power consumption of the system has to be taken into account. As reviewed in Chapter 2.1 and according to Kouzbary, Abu Osman, Kouzbary, Shasmin, and Arifin (2020), the selected motor for the application is a PMSM motor.

In this section, preliminary calculations with regards to the selection of the appropriate battery size for the prosthesis, given the design constraints, will be performed.

3.3.1 Assumptions

When selecting an appropriate battery for the system, a number of assumptions have to be considered:

1. Power consumption comes primarily from motor and inverter system, since other components use negligible power. Based on the datasheet of the MPU6050 sensor, the device consumes a maximum power of 12 x10^{-3} W (InvenSense, 2013).
2. The motor is considered a torque source mimicking joint torque (Tucker et al., 2015), hence, power usage varies with ankle moment during gait.
3. Parameters are based on male subjects since the latter use relatively more power at the ankle than female subjects (Rowe, Beauchamp, & Wilson, 2021).
4. Motor is considered idle during swing phase (40%) of gait.

3.3.2 Preliminary Calculations

Selecting a battery size for the application involves determining the voltage and current at which the battery operates as well as the total power capacity that the battery can hold with respect to time.

The first step is to determine the overall running time of the system. This is achieved using the number of steps the system is rated for, multiplied by the time taken to complete a complete gait cycle. A normal person in Malaysia has a stride time of approximately 1.21s (±0.36) according to data collected by Chong Yu, Lau Yee, Teh Chun, and Yunus (2015). The total walking time, T_{walk}, of the prosthesis is as given below:

$$T_{walk} = Number\ of\ steps * time\ taken\ for\ 1\ stride$$

$$T5k_{walk} = 5{,}000 * (1.21 \pm 0.36)\text{s} = 6050s\ (\pm 1800) = 1.7\ \pm 0.5\ h$$

$$T10k_{walk} = 10{,}000 * (1.21 \pm 0.36)\text{s} = 12{,}100s\ (\pm 3600) = 3.36\ \pm 1\ h$$

According to Amatya, Salimi Lafmejani, Poddar, Sridar, and Sugar (2019), a 74 kg adult with normal gait has a maximum ankle moment of about 96.2 Nm when the ankle angle is about 17°. Figure 3.1 below shows the ankle parameters for a healthy adult during gait as determined by Amatya et al. (2019).

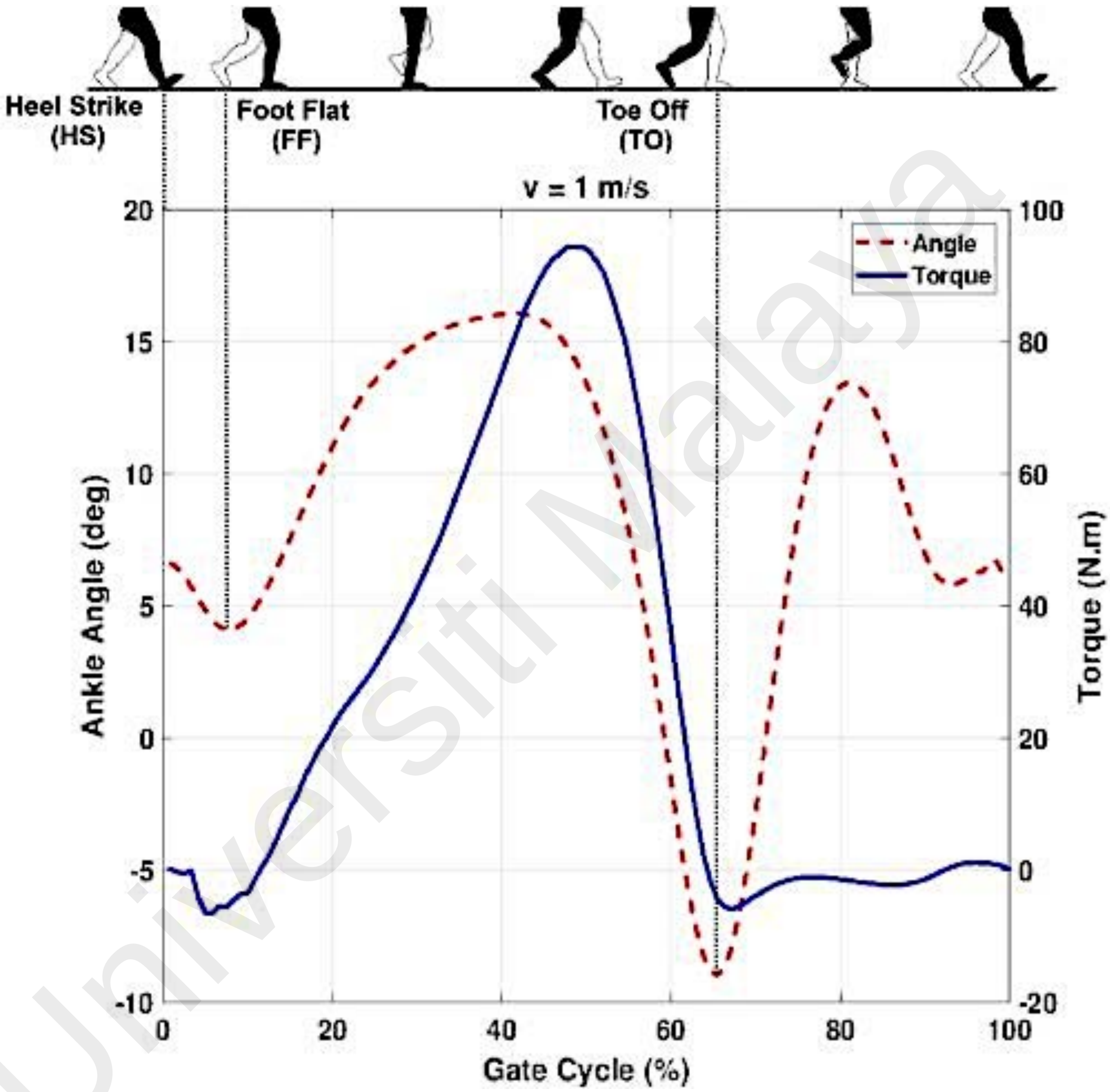

Figure 3.1: Ankle parameters during gait of healthy adult (Amatya et al., 2019)

The total mechanical power, P, required by motor during 1 gait cycle is the sum of the product of motor torque, T, and angular speed, ω, of the motor at different points during the cycle, and is calculated as follows:

$$P = \sum (T * \omega)$$

The gait cycle is divided into 4 segments to represent ankle moment and angle at different phases of gait. These segments are: (1) heel strike to foot flat, (2) foot flat to heel off, (3) heel off to toe off, and (4) swing phase. The ankle angle during 1 gait cycle ranges from -8° to 17° (Amatya et al., 2019). The total rotation of the ankle during one section of the gait cycle is given by:

$$Total\ Rotation = Ankle\ angle_{final} - \ Ankle\ angle_{initial}$$

The gait cycle is assumed to take 1.21s (±0.36), as previously mentioned, and the stance phase is roughly 65% of the gait cycle. The angular speed is given by:

$$\omega = 2\pi f\ = 2 * \pi * \left(\frac{Rotation\ \ of\ ankle\ in\ radians}{duration\ of\ gait\ segment}\right)$$

The total motor power required for 10,000 steps, therefore, is:

$$P_{10k}\ \ = P * T_{walk}$$

The inverter used in the RoMicP® prosthesis is a GaNFET by Texas Instrument (TI) with product ID LMG5200 and maximum input power ratings of 80V and 10A.

Hence, the total battery capacity required to power the system for 10,000 steps would be the sum of the total motor power and the total inverter power, as given below:

$$Battery\ capacity\ \ = P_{10k} + \ P_{Inverter}$$

As previously discussed in Chapter 2.2, the battery type suitable for this application is lithium-based. From the vendor datasheet, the total weight and price of the required battery can be obtained.

3.4 Analysis of power consumption

Once the battery capacity required for the system is determined, the system can be simulated to determine the power consumption, and hence the efficiency, of the inverter and motor system. To have a baseline to compare future results with, a 3-phase inverter, powered by the battery previously determined, and connected to a 3-phase load is used. Figure 3.2 below shows the proposed schematic of the system to be simulated.

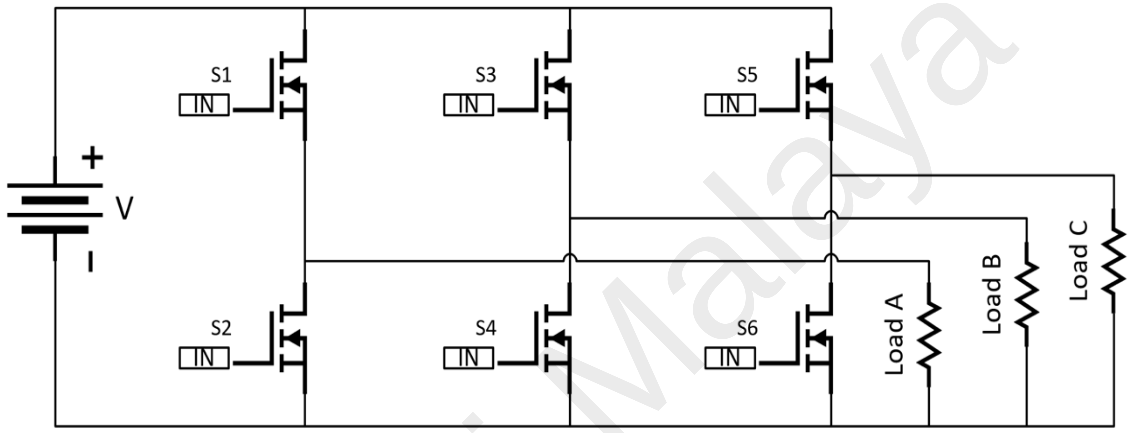

Figure 3.2: Three-phase MOSFET inverter schematic

The system shown in Figure 3.2 shows 3 sets of 2 MOSFETs, each connected to a load (A to C) representing one phase of a 3-phase PMSM motor and powered by a battery. In order to generate a proper AC output for each phase, the MOSFETs have to be switched at specific intervals from one another.

3.4.1 Inverter switching

No two vertical switch pairs (for example: S1 and S2 in Figure 3.2) should be ON at the same time. In practice, the switching is done through signals from a microcontroller. In the simulation, the same can be achieved by applying pulses to the switches, labelled "IN" in Figure 3.2. The general timings used to switch S1 and S2 are shown in Figure 3.3 below.

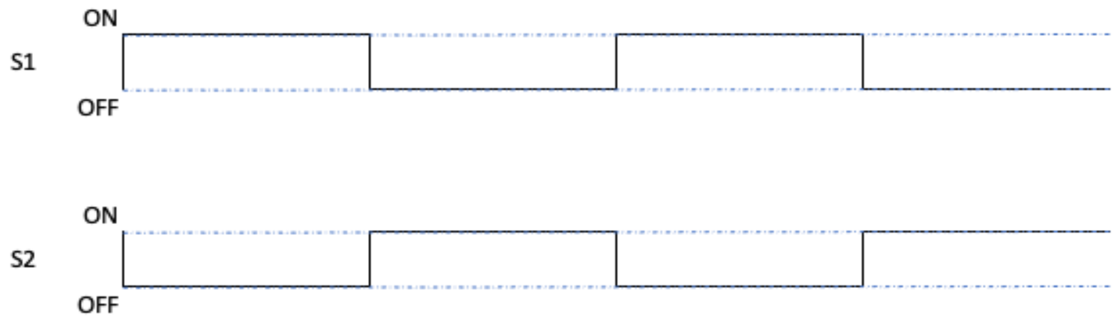

Figure 3.3: Switch timings

As shown in Figure 3.3, the switches have opposing polarity at all times, i.e., when S1 is on, S2 is off, and vice-versa. To increase the efficiency of the system and obtain an output closer to an ideal 50Hz sine wave, the switched inputs are pulse-width modulated at a frequency of 40 kHz. This is achieved by comparing a 40 kHz triangular wave and a superimposed 50 Hz sine wave.

3.4.2 Simulation system design

The datasheet of the LMG5200 describes the device as half-bridge, implying that it internally consists of 2 MOSFETs, driven by a proprietary GaN driver (Texas Instruments, 2018). Figure 3.4 below shows the simplified block diagram of the device as described by TI.

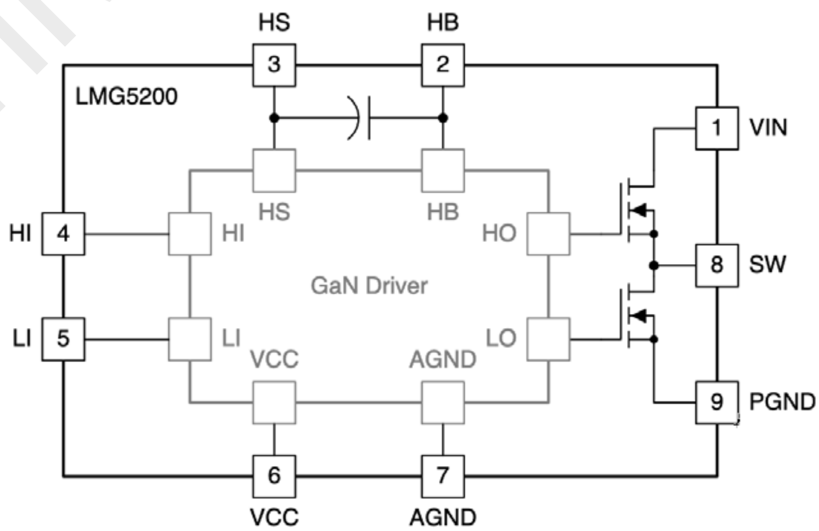

Figure 3.4: Simplified block diagram of the LMG5200 (Texas Instruments, 2018)

The positive terminal of the battery (+24V) will be connected to pin 1 (VIN) on the LMG5200 as shown in Figure 3.4 above. Pins 7 (AGND) and 9 (PGND) will be grounded while pin 6 (VCC) will be connected to a 5V supply as proposed in the datasheet. The high-side of the GaNFET will be switched through pin 4 (HI) and the low-side will be switched via pin 5 (LI), while the output will be measured through pin 8 (SW).

Since the LMG5200 is a proprietary technology, the only available information on the device is available through TI, which provided a working schematic of a single-phase switching circuit, as shown in Figure 3.5 below, for their own TINA software for circuit simulation.

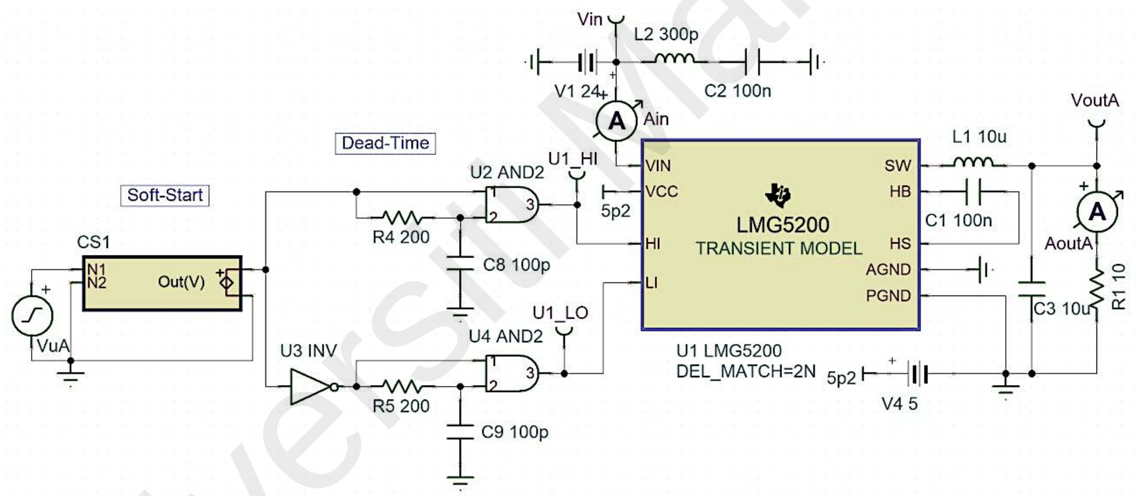

Figure 3.5: Simulation schematic for TINA software

The switching of the LMG5200 will be controlled through device CS1 on the left of Figure 3.5, and the power input of the device will be measured through Vin (voltage) and Ain (current) while the output power will be measured across the output load R1 through VoutA (voltage) and AoutA (current) for each phase. To measure the overall power input, output and consumption, the 3-phase circuit will be designed as shown in APPENDIX B.

3.5 Multi-level inverter feasibility

As highlighted in Chapter 2.4 and Chapter 2.5, increasing the levels in the inverter system should systematically improve the performance of the AC signal. However, due to practical constraints there are limits to the number of levels that can be implemented in order to achieve a feasible compromise between performance, power consumption and overall size of system.

To examine the feasibility of employing a multi-level inverter in the RoMicP® prosthesis, the simulated model from Chapter 3.4 will be extended to multiple levels and simulated to measure the output and power consumption. Figure 3.6 below shows a proposed five-level MLI with three-phase outputs.

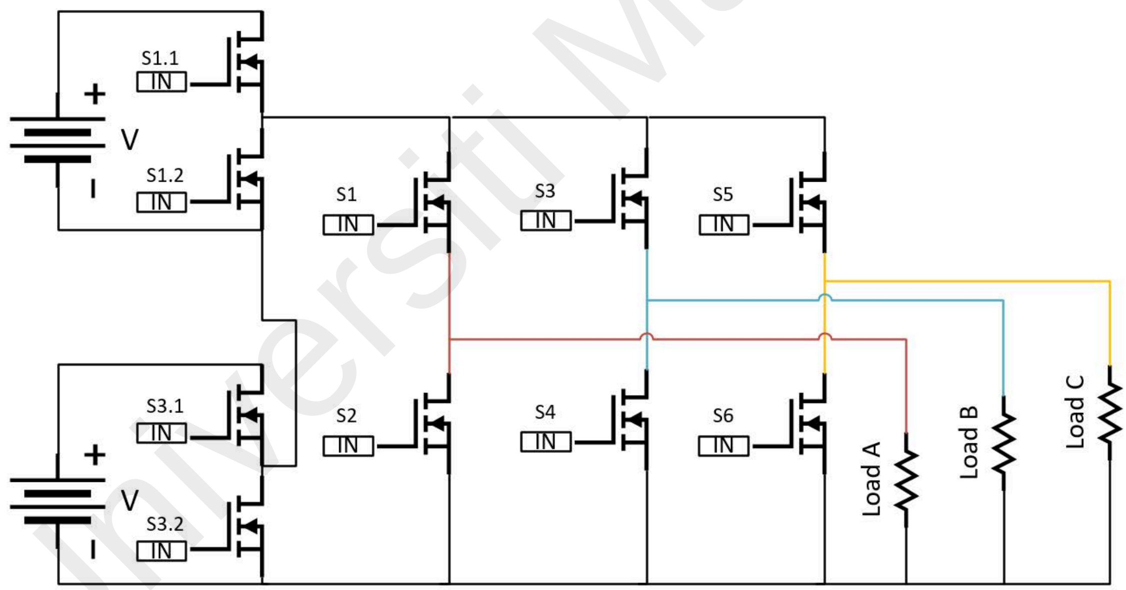

Figure 3.6: Three-phase five-level multi-level inverter

The proposed system consists of 6 half bridges in 2 stages: the first stage consists of 2 cascaded half bridges and the second phase consists of 3 parallel bridges connected to a load. Colored wires red, blue, and yellow each represent one output phase through resistive loads A, B, and C respectively. The supply, V, through each H-bridge represent half ($V_{Battery}/2$) of the total battery power calculated in Chapter 3.3.2.

3.6 Summary

In Chapter 3, the methodology of the project has been discussed in 3 stages to fulfil the objectives as summarized in Figure 3.7 below.

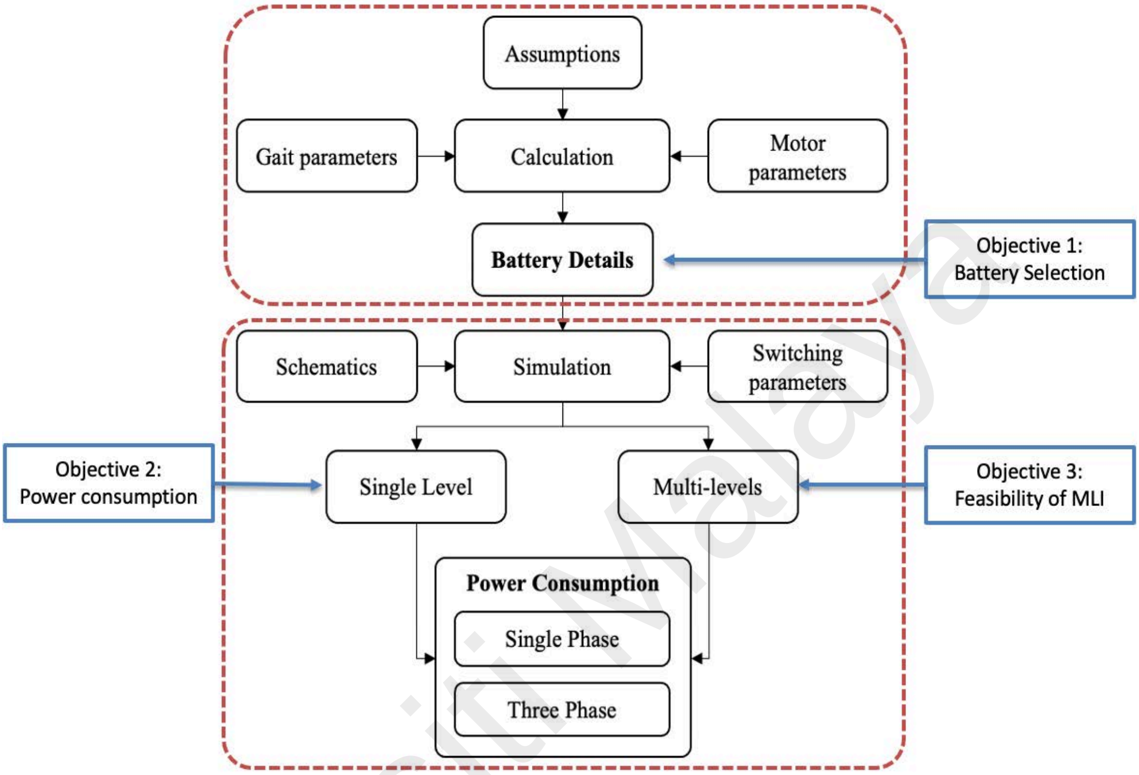

Figure 3.7: Research design summary flowchart

The battery parameters will be calculated using discussed gait parameters, assumptions, and motor parameters. The former will then be used in conjunction with the proposed schematics and switching inputs to simulate both single- and multi-level inverter circuits using the LMG5200 IC. In both cases, the power consumption of the system for a single phase as well as three phases will be measured and assessed using the root mean square (rms) values of voltage, current, and power.

CHAPTER 4: RESULTS

4.1 Introduction

In this chapter, relevant results obtained after calculations and running the simulations explained in the previous chapters will be shown and further investigation will be carried out to determine the overall power consumption and efficiency of the system while ensuring the system conforms to the design criteria of maximum weight of 2.5kg and a maximum of 10,000 steps per day for the prosthesis.

4.2 Battery Selection

The calculations for each segment of the gait cycle are tabulated in Table 3.2 below. Gait parameters such as ankle angle and moment were obtained from Figure 3.1 and other parameters were calculated as mentioned in Chapter 3.3.2.

Table 4.1: Power calculation for different gait segments

	Heel strike to Foot flat	Foot flat to Heel off	Heel off to Toe off
% of gait cycle	10	40	15
Time, T (s)	0.121 ± 0.036	0.484 ± 0.114	0.1815 ± 0.054
Ankle Rotation (°)	3 ± 1	13 ± 1	25 ± 1
Ankle Rotation (rad)	0.0523 ± 0.02	0.2269 ± 0.02	0.4363 ± 0.02
Rotation frequency, f (rad/s)	0.4322 ± 0.48	0.4688 ± 0.25	2.4039 ± 0.30
Angular velocity, w (rad/s)	2.7158 ± 3.0	2.9456 ± 1.6	15.1039 ± 1.9
Ankle Moment (Nm)	-7 ± 2.5	96.2	-7 ± 2.5
Adjusted Moment (Nm)	6.7635 ± 2.4	92.95	6.7635 ± 2.4
Motor Torque (Nm)	6.7635 ± 2.4	92.95	6.7635 ± 2.4
Power (W)	18.37 ± 1.16	273.79 ± 1.6	102.16 ± 0.13

From Table 4.1 above, the total power spend during one gait cycle can be approximated as follows:

$$Total\ power\ per\ cycle = \Sigma\,\mathrm{Power} = 394.32 \pm 2.89\ \mathrm{W}$$

Using the power formula for a typical 3-phase AC motor, with a power factor of 1 due to resistive load, the electrical power input to the motor is given by:

$$Motor\ Power_{in} = \frac{Motor\ Power_{out}}{power\ factor * \sqrt{3}} = \frac{394.32 \pm 2.89}{1 * \sqrt{3}} = 227 \pm 1.67\ W$$

The input to the motor is provided by the inverter, which is powered by the battery. The power efficiency of the LMG5200 is given as 98.5% by Texas Instrument, therefore the total theoretical power required to power the system is given by:

$$Total\ Power_{in} = \frac{100 * 227 \pm 1.67}{98.5} = 230 \pm 1.7\ W$$

Considering the minimum steps to be 5,000 and the maximum to be 10,000, according to the design criteria, and the time for which power is required in the motor,

$$Min\ usage\ time = time\ for\ stance\ phase * 5k = 3932 \pm 0.2\ s \approx 1.1\ h$$

$$Max\ usage\ time = time\ for\ stance\ phase * 10k = 7865 \pm 0.2\ s \approx 2.18\ h$$

$$Min\ input\ power\ required = 227 \pm 1.67\ W * 1.1\ h = 250 \pm 4\ Wh$$

$$Max\ input\ power\ required = 227 \pm 1.67\ W * 2.18\ h = 495 \pm 4\ Wh$$

$$Min\ rated\ battery\ capacity = \frac{250 \pm 4\ Wh}{24\ V} = 10 \pm\ 0.2\ Ah$$

$$Max\ rated\ battery\ capacity = \frac{495 \pm 4\ Wh}{24\ V} = 20 \pm\ 0.2\ Ah$$

The battery required for this application should therefore fulfill the specifications shown in Table 4.2 below.

Table 4.2: Required battery specifications

Parameter	5k Steps (Min.)	10k Steps (Max.)
Usage Time	1 h 06 min	2 h 10 min
Voltage (V)	24	24
Rated Power Capacity (Ah)	10 ± 0.2	20 ± 0.2
Energy Capacity (Wh)	250 ± 4	495 ± 4

4.3 Simulation Results, Power Consumption & Efficiency

In this section, the results of the simulations that have been performed are presented as well as the power consumption of the simulated inverter systems.

4.3.1 PWM Switching

To obtain the PWM signal to switch the GaN-FET devices in the TINA-TI software, two superimposed signals consisting of a triangular wave of frequency 40kHz and a sine wave of frequency 50Hz are used. The 2 signals are processed through a comparator to produce the PWM signal shown in red in Figure 4.1 below. The PWM signal shows a set of pulses that switch between 0V and 5V and vary in time based on the amplitudes of the compared signals: as the amplitude of the sine wave increases, the 5V pulse width increases, and as the amplitude reduces, the 0V pulse width increases.

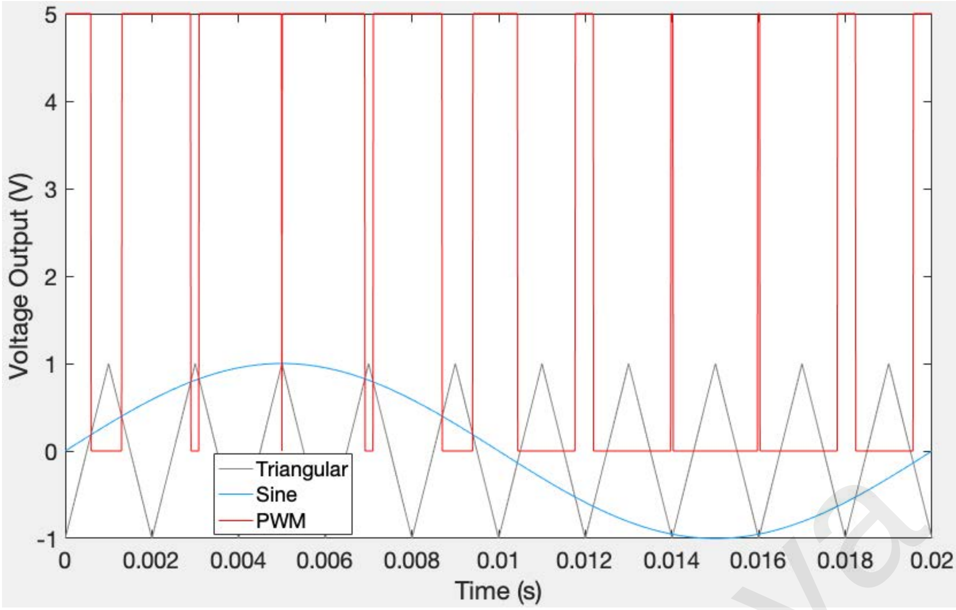

Figure 4.1: PWM switching results

Running the simulations with these frequencies require large computation power. Hence, to reduce the simulation time for complex designs, the switching frequency was reduced to 10kHz when necessary.

4.3.2 Single-Phase Single-Level Inverter Simulation

Running the simulation of the original schematic design provided by TI shown in Figure 3.5 from Chapter 3.4 for a duration of 50ms, the following behavior was observed.

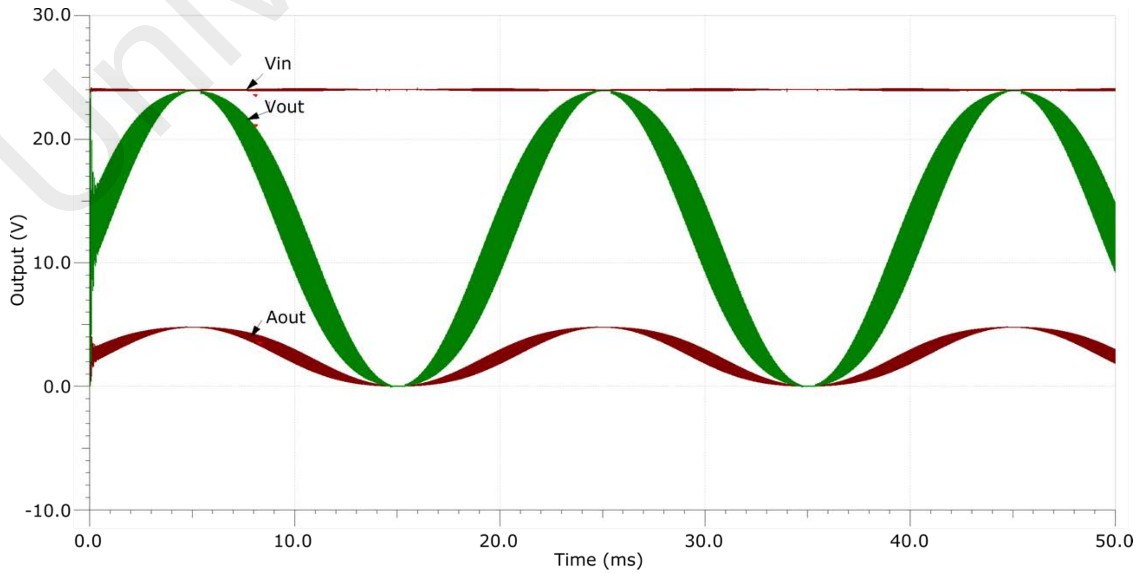

Figure 4.2: Simulation results of original TI schematic

As Figure 4.2 shows, the output of the LMG5200 oscillates between 0V to 24 V at 50Hz. This is however not the expected behavior of the device as there are also oscillations within the signal which may be due to the presence of an LC filter at the output. By removing the filter from the schematic, the simulation was run once more for 50ms, and the output behavior for 1 cycle is shows in Figure 4.3 below.

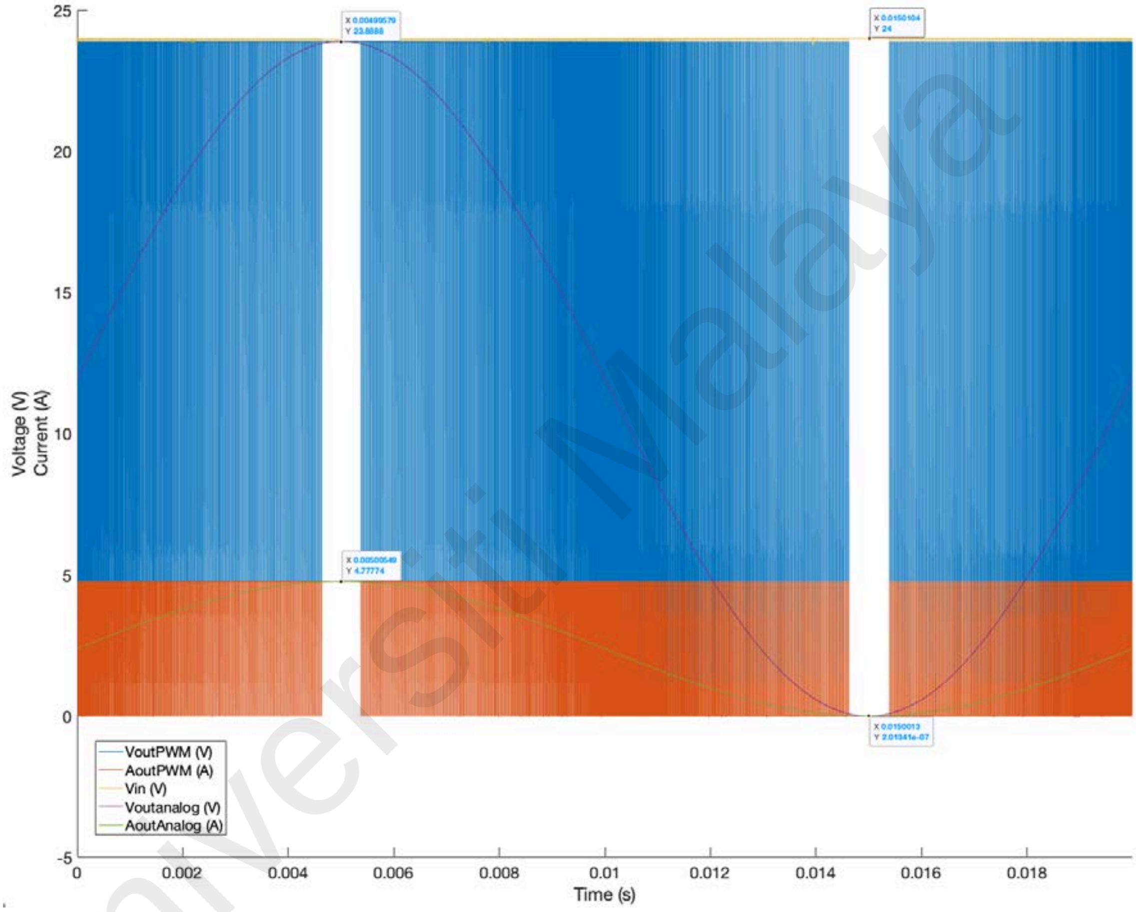

Figure 4.3: Simulation results of 1-phase unfiltered inverter circuit

From Figure 4.3, it can be observed that the input (Vin, shown in yellow) was 23.98 ± 0.02 V, while the output voltage (VoutPWM, shown in blue) switched between 1.46 ± 5.6 x10^{-5} V and 23.89 ± 0.0004 V, and the current at the output (AoutPWM, shown in red) switched between 2.93 ± 1.12 x10^{-5} A and 4.78A ± 0.0001.

The power consumption and efficiency of the single-phase, single-level inverter is given in Table 4.4 below.

Table 4.3: Power consumption & efficiency of one-phase single-level simulation

	Rms Voltage (V)	Rms Current (A)	Power (W)
Input	23.9761	3.3782	80.9961
Output	16.8751	3.3750	56.9534
Efficiency (%)			70.31%

The power generated by the battery at the input was 80.9961W and the power consumption of the system was 56.9534W. The overall efficiency of the single-phase, single level inverter system was hence 70.31%.

4.3.3 Three-Phase Single-Level Inverter Simulation

The circuit in 4.3.3 was then expanded to a three-phase configuration (refer to APPENDIX B for full schematic), connected to a delta resistive load, with the 3 LMG5200 connected in parallel to the 24V power supply. Each IC was switched with a similar PWM signal as shown in section 4.3.1, shifted by 120° to each other.

Input voltage was measured from the same node connecting all 3 ICs and input current to each IC was measured separately. Output voltages and currents were measured at the output of the ICs, and phase voltages were measured between the 3 output lines.

Figure 4.4 below shows the simulation results of the three-phase single-level inverter system, with the phase voltages shown in blue and phase currents shown in yellow.

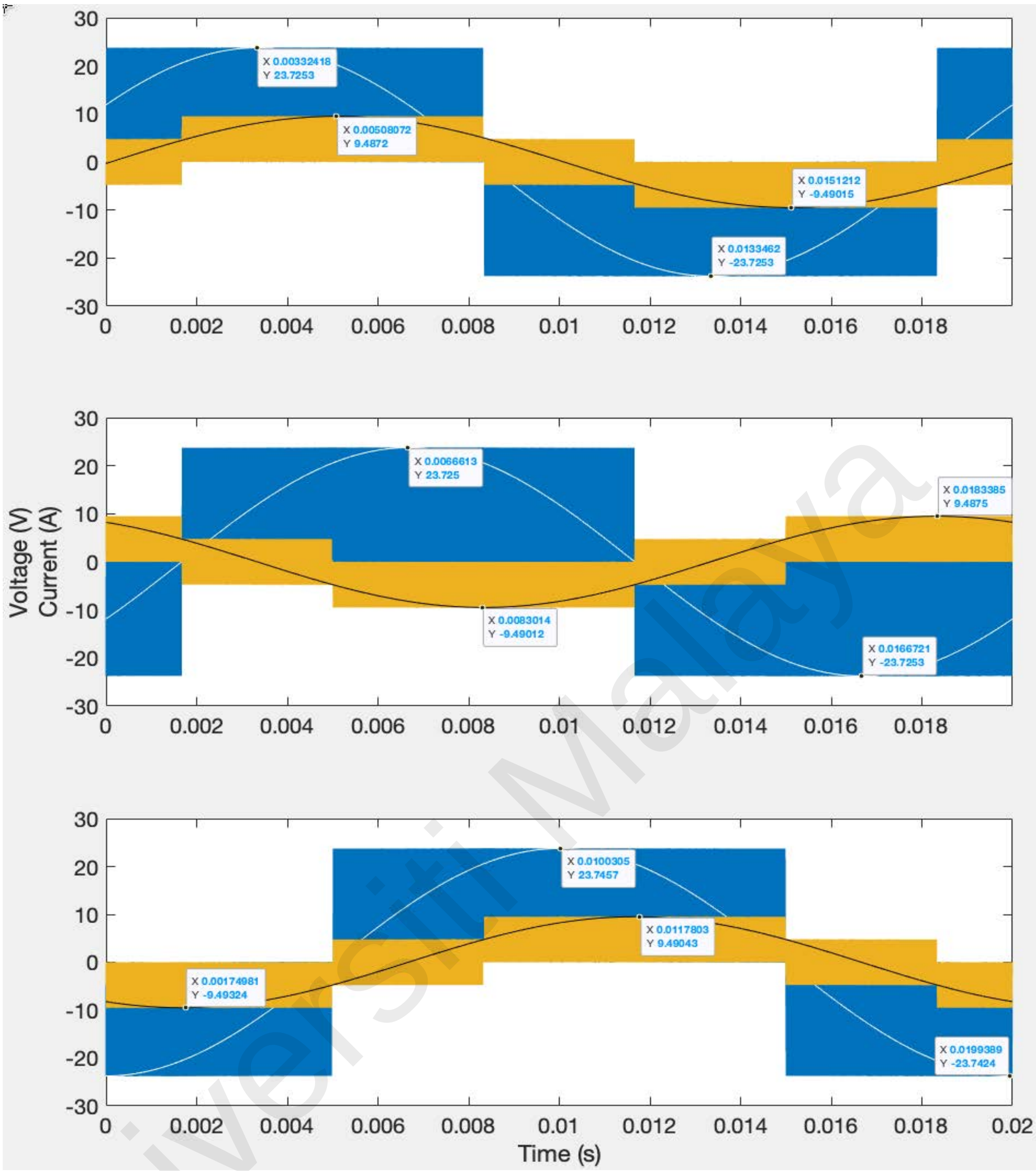

Figure 4.4: Simulation results of 3-phase single-level inverter circuit

The phase 1 output voltage varied between a maximum of +23.7468V and a minimum of -23.7467V while the current varied between +9.4965A and -9.4963A. The output of phase 2 varied between +23.7467V and -23.7468V while the current varied between +9.4970A and -9.4963A. Finally, the voltage across phase 3 varied between ± 23.7468V while the current varied between +9.4965A and -9.4975A.

The power consumption and efficiency of the three-phase single-level inverter simulation system was calculated as shown in Table 4.6 below.

Table 4.4: Power consumption & efficiency of three-phase single-level simulation

		Rms Voltage (V)	**Rms Current (A)**	**Power (W)**
Phase 1	**Input**	23.9232	4.2691	102.1302
	Output	16.8667	6.0380	101.8414
	Efficiency			99.72%
Phase 2	**Input**	23.9232	4.2684	102.1129
	Output	16.8659	6.0381	101.8388
	Efficiency			99.73%
Phase 3	**Input**	23.9232	4.2688	102.1239
	Output	16.8693	6.0363	101.8279
	Efficiency			99.71%
Overall Efficiency (%)				**99.72%**

Using the current and voltage values from Figure 4.4, the rms voltage, current and power for each phase were calculated. Phase 1 used 102.1302W of power to generate 101.8414W, hence yielding an efficiency of 99.72%. Phase 2 used 102.1129W of power to generate 101.8388W, hence yielding an efficiency of 99.73%. Finally, phase 3 used 102.1239W of power to generate 101.8279W, hence yielding an efficiency of 99.71%. The overall efficiency achieved by the single-level three-phase inverter simulation was calculated to be 99.72%.

4.3.4 Three-Phase Five-Level Inverter Simulation

To test the feasibility of a MLI, a 5-level three-phase inverter was simulated using the LMG5200. To achieve 5-levels for one phase, 8 (from 2(n-1), where n is the number of levels) FET devices were required. The schematic used for 1 phase is shown in Figure 4.5 below (refer to APPENDIX C for large-scale image, and APPENDIX D for three-phase schematics).

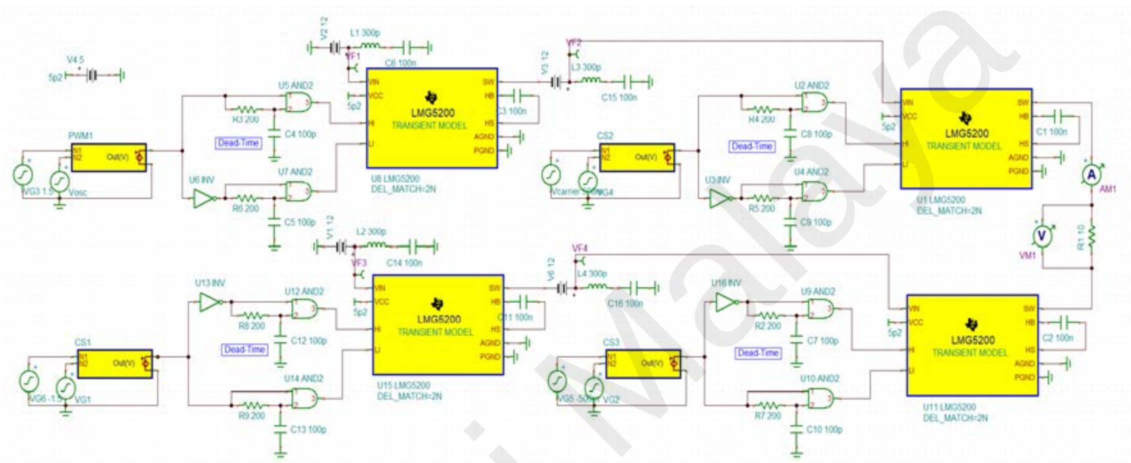

Figure 4.5: One-phase five-level MLI schematics

The changes in the schematic shown in Figure 4.5 above include the addition of the second voltage source between the output of the first inverter level and the power input of the second inverter level. The simulation was run for one cycle of 50Hz with a switching frequency of 10kHz due to the limited hardware resources to compute the simulation results. The results were then measured across the outputs for each phase to determine the power output and efficiency using this MLI topology.

Figure 4.6 below shows the output voltages and currents for each phase of the MLI simulation. Each phase is represented by a specific color: blue, green, and yellow. The results can be observed to be as expected from a 5-level MLI.

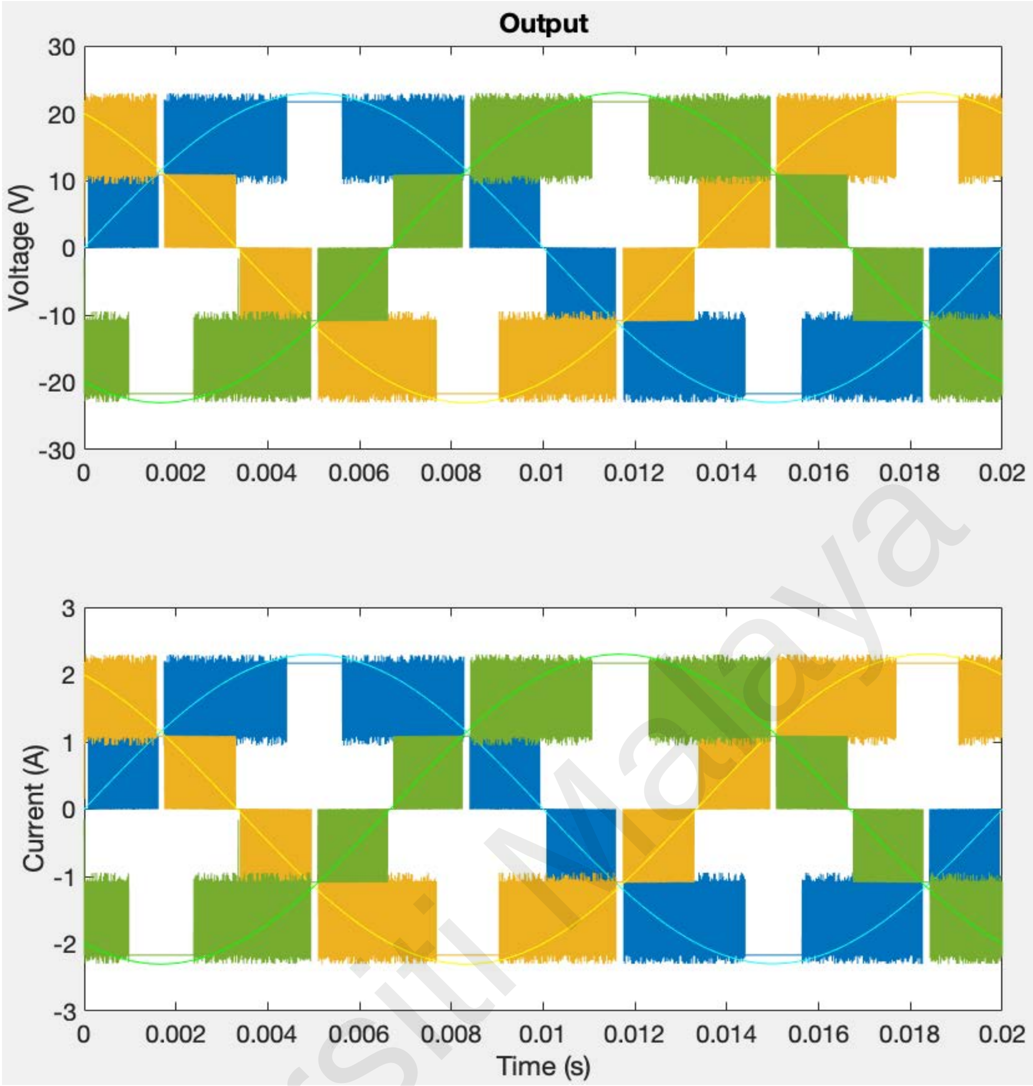

Figure 4.6: 3-phase 5-level MLI simulation outputs

The results in Figure 4.6 above show the 3-phases at 120° from each other. The voltage and current levels for each phase are extracted in Table 4.7 and 4.8 below respectively.

Table 4.5: Voltage levels of simulated MLI

	0V	V	2V	-V	-2V
Phase 1	0	10.86	21.70	-10.86	-21.70
Phase 2	0	10.86	21.70	-10.86	-21.70
Phase 3	0	10.86	21.70	-10.86	-21.70

Table 4.6 shows that all 3 phases settle at similar levels of 0V, ± 10.86V, and ± 21.70V.

Table 4.6: Current levels of simulated MLI

	0A	A	2A	-A	-2A
Phase 1	0	1.09	2.17	-1.09	-2.17
Phase 2	0	1.09	2.17	-1.09	-2.17
Phase 3	0	1.09	2.17	-1.09	-2.17

Table 4.7 shows that all phases settle at similar current levels of 0A, ± 1.09A, and ± 2.17A.

The power consumption and efficiency of the three-phase five-level inverter simulation system was calculated as shown in Table 4.8 below.

Table 4.7: Power consumption & efficiency of three-phase five-level simulation

		Rms Voltage (V)	Rms Current (A)	Power (W)
Phase 1	**Input**	55.3433	3.4422	45.6750
	Output	16.441	1.6441	27.0308
	Efficiency			59.18%
Phase 2	**Input**	55.3911	3.4343	45.6201
	Output	16.4747	1.6475	27.1415
	Efficiency			59.49%
Phase 3	**Input**	55.4524	3.4424	45.7597
	Output	16.5289	1.6529	27.3205
	Efficiency			59.70%
Overall Efficiency (%)				**59.46%**

Table 4.8 shows an average rms voltage of 16.48 ± 0.04V and rms current of 1.648 ± 0.004A for each phase, and overall efficiency of 59.46% for the 5-level topology used.

4.3.5 Harmonic Distortion

When using PWM switching, one important parameter to look into is the harmonic distortion between the harmonic signals and the fundamental signal frequency (50Hz in this case). The TINA-TI software provides a built-in tool to analyze harmonic distortion using Fourier transform, which was manually tuned for 11 harmonics using rms values for each output. Table 4.9 below shows the results obtained for harmonic distortion of the single-phase, three-phase single-level and three-phase five-level circuit simulations.

Table 4.8: Harmonic distortion of outputs

	Harmonic Distortion (%)			
	Phase 1	**Phase 2**	**Phase 3**	**Average**
1-phase, single-level	2.9385			2.9385
3-phase, single-level	2.2575	2.1082	2.086	2.1506
3-phase, five-level	0.8314	0.8196	0.8126	0.8212

Table 4.9 shows that the harmonic distortion reduced by 27% from one-phase to three-phase single-level simulation and by 62% from three-phase single-level to multilevel.

4.4 Summary

In Chapter 4, the calculations and results pertaining to the battery specifications were presented, followed by some available models that fulfil the requirements. Moreover, the simulation results of a single-phase single-level, three-phase single-level, and three-phase five-level inverter system were presented and analyzed, and their power consumption and efficiency calculated. Finally, the harmonic distortion that occur at the output of each simulation were also presented.

CHAPTER 5: DISCUSSION

5.1 Introduction

In this chapter, the calculations performed, and results obtained in Chapter 4 will be discussed. Moreover, an in-depth analysis of the project will be performed, and some limitations discussed.

5.2 Battery Selection

To select the appropriate battery model for the prosthesis, a few suppliers have been surveyed (see APPENDIX A) for available custom-made lithium batteries that can fulfil the calculated specifications. By using the ratings of each cell and combining them to meet the calculated specifications, the total weight and price of each battery pack can be estimated as shown in Table 5.1 below.

Table 5.1: Total number of cells required to fulfil battery specifications

	ID (from APPENDIX A)	1	2	3
10 Ah Capacity	Number of Cells Required	7	1	7
	Total Weight (g)	n/a	1650	1400
	Total Price (USD)	245.00	573.95	222.60
20Ah Capacity	Number of Cells Required	13	2	13
	Total Weight (g)	n/a	3300	2600
	Total Price (USD)	455.00	1147.90	413.40

Table 5.1 above shows that battery type 1 and 3 require 7 cells to achieve the minimum capacity of 10Ah at 24V and cost USD 245 and 222.60 in total respectively, while type 2 only requires 1 pack to achieve the same but at a higher price of USD 573.95. While

weight data is not available for type 1, the total weight of a 10Ah battery pack for the prosthesis using type 3 would be 1.4 kg and type 2 has a total weight of 1.65 kg.

To achieve the maximum rating of 20Ah, 13 cell units would be required from types 1 or 3 with a total cost of USD 455.00 and USD 413.40 respectively while type 2 would require only 2 units at a total price of USD 1147.90. The weight of type 1 was not available, but the total required weight of the type 2 battery pack is estimated at 3.3 kg while that of type 3 is 2.6 kg.

Hence, the battery model that can be recommended for the RoMicP® that match the design requirements is the PL-9059156-1C from AA Portable Power Corp which can achieve a total of 5,000 prosthesis steps in a day (total daily steps of 10k by patient) at a price of USD 222.60 and a total weight of 1.4kg.

5.3 Inverter Power Consumption

In order to accurately assess the performance of the inverter system, the simulation model of the LMG5200 IC from Texas Instruments was sourced from the manufacturer website and simulated in their proprietary TINA-TI software. The original simulation file was modified to be used as a DC to AC inverter. The "soft-start" component that delayed the circuit response was replaced with a switching device for the IC and the inductor-capacitor (LC) filter at the output was removed to study the maximum power usage of the system. The circuit contained a "dead-time" control sub-circuit that helped eliminate dead-band issues that occur in inverter switching and was thus retained during analysis.

Running the simulation on only 1 LMG5200 device showed that with a battery of 23.98 ± 0.02 V producing 80.99W of power, an output power of 56.95W could be achieved. Therefore, the overall efficiency of the inverter system in this case would be

70.31%, indicating high power loss which will mostly produce heat in the system, thus requiring additional cooling systems to maintain working conditions.

To improve the power consumption, and hence the efficiency, a three-phase inverter system was simulated by adding 2 additional LMG5200 ICs that were then switched with a phase shift of 120° for the second phase and 240° for the third. The results showed that for an average input DC power of 102.1W at 23.92V, the average rms power generated by the system was 101.8W at 16.86Vrms (or 23.86V peak-to-peak). The efficiency of the system is hence drastically improved to 99.72%, implying that the losses from the system are reduced.

The results from the simulation show that using the LMG5200 could have a positive effect on the power consumption of the prosthesis and as such improve the longevity of the electronics of the prosthesis. Moreover, less energy will be lost as heat and thus only passive cooling might be enough. Another benefit of using this IC would be the need for a small circuit-board due to the small size of the former.

5.4 Feasibility of Multi-Level Inverter

It has been reported in the literature (see Chapter 2) that using multi-level inverter systems can help overcome limitations of single-level inverters. For example, the output waveforms are closer to the desired sinusoidal signal, therefore enhancing the behavior of the connected motor. A MLI was hence simulated to compare with the three-phase single-level inverter to determine whether the setup is feasible.

There are numerous topologies implemented for multi-level inverters, each having its pros and cons. For this experiment, the typical H-bridge configuration could not be implemented possibly because of the internal proprietary working of the simulated IC and simulation software that could not perform the simulation calculations. Hence, a different topology was implemented, as shown in the schematic diagram in Figure 5.1 below.

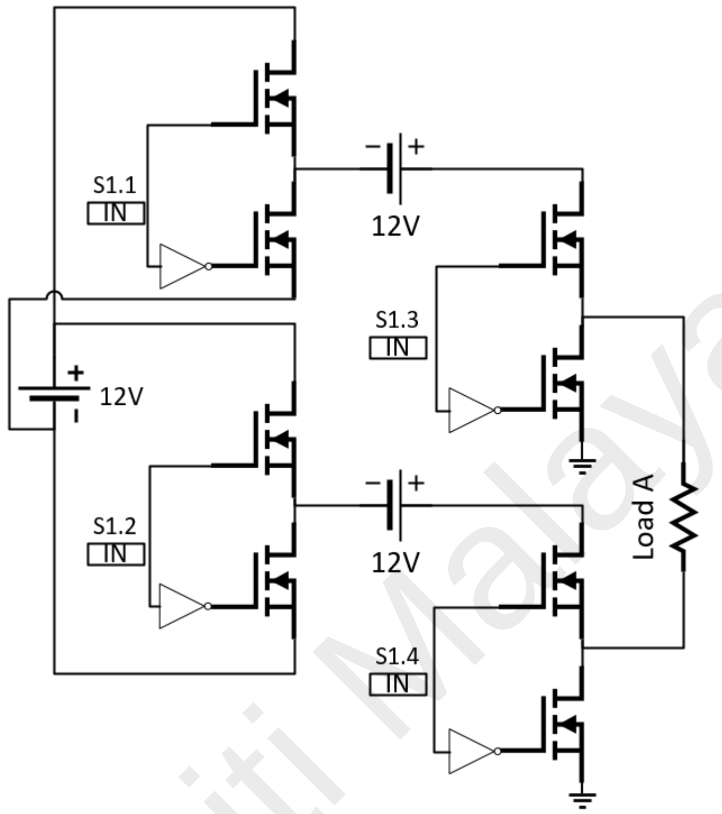

Figure 5.1: Simulated five-level MLI topology

Figure 5.1 shows 1 phase of the topology used where the first level on the left consists of 2 LMG5200 ICs powered by a 12V battery and switched with PWM at S1.1 and S1.2, and the output of each IC was fed to a 12V battery to supply the second inverter level. The outputs were then measured across load A. The same was repeated for phase 2 and 3 and the whole circuit was simulated.

Results showed that for a total combined average input of 45.68W, the average power output was 27.16W at rms voltage of 16.4V (or 23.82V peak-to-peak). While the output voltage was as expected, and the waveform produced was a five-level PWM AC output, the efficiency of the five-level inverter system was reduced to 59.46%, a drop of 40% from single-level.

It was also observed that because of the more accurate sinusoidal representation, there was less harmonic distortion in the five-level system compared to single-level by 62%. This shows that there are potential benefits of implementing MLIs. However, due to the large drop in efficiency, this particular five-level topology cannot be recommended for implementation over the single-level inverter.

5.5 Limitations

Although the calculations performed to determine the battery specifications represent the worst-case scenario when using the prosthesis, parameters such as battery discharge rate, battery-life, temperature, and other power losses were not taken into account. To gauge the actual battery requirements, further lab tests will be required based on physical and chemical parameters of selected batteries to confirm the specifications.

The LMG5200 IC is a proprietary chip from TI and hence has to be used as-is and the internals cannot be fully understood. The only way to understand its behavior was to observe the input and output by varying certain parameters. This could possibly be one of the major sources of error and efficiency loss when designing the MLI as the pins are programmed to act as either input or output. However, the actual IC might allow certain pins to act as both inputs and outputs, thus altering its behavior.

Furthermore, the only switching method employed in the simulation was the PWM method as it is the most commonly used type of switching method. This project did not explore the performance of the system when other advanced switching methods are used.

Finally, this work does not investigate the effects of digital or analog filters on the circuit which might impact the power input and output and hence performance.

CHAPTER 6: CONCLUSION AND FUTURE WORKS

6.1 Conclusion

The first objective described in this project was to investigate suitable battery specifications that would allow the prosthesis to operate within its design constraints. By means of the necessary assumptions and calculations, 2 battery models were found to fulfil the design specifications; the first was the PL-9759156-7S by AA Portable Power Corp weighing 1.65kg at USD 573.95, and the second was the PL-9059156-1C by AA Portable Power Corp weighing 1.4kg and costing USD 222.60. Both batteries can provide power for a total of 5,000 steps per day using the prosthesis.

The second objective was to analyze the power consumption and efficiency of the inverter system using the LMG5200 through simulations. The inverter was simulated using the TINA-TI software and it was found that the average power consumption of a three-phase single-level inverter setup was 101.84W and the efficiency was at 99.72% when simulated at 40kHz switching frequency.

The final objective was to determine if using a multi-level inverter setup is feasible and what the impact would be on the efficiency of the system. By simulating a five-level inverter system and comparing it with the single-level three-phase results, it can be concluded that using the topology proposed in this project a MLI would not be recommended since the efficiency drops from 99.72% to 59.46%. However, it should be noted that using a MLI produces harmonic distortions that are 62% lower than a single-level inverter, indicating better resemblance to a pure sinusoidal signal.

6.2 Future Works

While this project investigated certain aspects of implementation of inverters in the RoMicP®, further study is required to improve understanding of the system and hence the performance of the latter.

One area of focus would include investigating the actual effects of the battery on the system and how discharge rate affects the power generated by the inverter and the performance of the motor.

Moreover, while PWM switching can achieve great results, there exist other advanced PWM switching methods such as Stepped wave, In-Phase Disposition, and other methods such as Space Vector Modulation, Space Vector Control or Selective Harmonic Elimination that may help reduce overall power consumption. Exploring the feasibility of these techniques could help increase the efficiency of the system.

As the results obtained suggest, the implementation of a multi-level inverter system may help to generate better signals for the motor to perform better. Hence, another area of focus might be to investigate various MLI topologies as well as increasing the levels from 5 to 7 or 9 and analyzing the behavior of the system.

While MLI can improve the output waveform, the effect of different digital or analog RLC filters should also be investigated in order to produce cleaner output for the motor.

REFERENCES

Al Kouzbary, M., Abu Osman, N. A., Al Kouzbary, H., Shasmin, H. N., & Arifin, N. (2020). Towards Universal Control System for Powered Ankle–Foot Prosthesis: A Simulation Study. *International Journal of Fuzzy Systems, 22*(4), 1299-1313. doi:10.1007/s40815-020-00855-4

Alishah, R. S., Nazarpour, D., Hosseini, S. H., & Sabahi, M. (2014). New hybrid structure for multilevel inverter with fewer number of components for high-voltage levels. *IET Power Electronics, 7*(1), 96-104. doi:10.1049/iet-pel.2013.0156

Amatya, S., Salimi Lafmejani, A., Poddar, S., Sridar, S., & Sugar, T. (2019). *Design, Development, and Control of a Fabric-Based Soft Ankle Module to Mimic Human Ankle Stiffness*.

Antivachis, M., Niklaus, P. S., Bortis, D., & Kolar, J. W. (2021). Input/output EMI filter design for three-phase ultra-high speed motor drive gan inverter stage. *CPSS Transactions on Power Electronics and Applications, 6*(1), 74-92. doi:10.24295/CPSSTPEA.2021.00007

Babaei, E., Alilu, S., & Laali, S. (2014). A New General Topology for Cascaded Multilevel Inverters With Reduced Number of Components Based on Developed H-Bridge. *IEEE Transactions on Industrial Electronics, 61*(8), 3932-3939. doi:10.1109/TIE.2013.2286561

Babaei, E., Farhadi Kangarlu, M., & Sabahi, M. (2014). Extended multilevel converters: an attempt to reduce the number of independent DC voltage sources in cascaded multilevel converters. *IET Power Electronics, 7*(1), 157-166. doi:10.1049/iet-pel.2013.0057

Bernatchez, J., Mayo, A., & Kayssi, A. (2021). The epidemiology of lower extremity amputations, strategies for amputation prevention, and the importance of patient-centered care. *Seminars in Vascular Surgery, 34*(1), 54-58. doi:10.1053/j.semvascsurg.2021.02.011

Chong Yu, Z., Lau Yee, C., Teh Chun, S., & Yunus, J. (2015, 1-4 Nov. 2015). *Development of normative human gait kinematics and kinetics database for Malaysian university students.* Paper presented at the TENCON 2015 - 2015 IEEE Region 10 Conference.

Derammelaere, S., Haemers, M., Viaene, J. D., Verbelen, F., & Stockman, K. (2016, 13-16 Nov. 2016). *A quantitative comparison between BLDC, PMSM, brushed DC and stepping motor technologies.* Paper presented at the 2016 19th International Conference on Electrical Machines and Systems (ICEMS).

Ding, X., Du, M., Zhou, T., Guo, H., & Zhang, C. (2017). Comprehensive comparison between silicon carbide MOSFETs and silicon IGBTs based traction systems for electric vehicles. *Applied Energy, 194*, 626-634. doi:10.1016/j.apenergy.2016.05.059

Ershad, N. F., & Mehrjardi, R. T. (2018, 8-9 Feb. 2018). *A low cost single-phase to three-phase power converter for low-power motor drive applications.* Paper presented at the 2018 IEEE Texas Power and Energy Conference (TPEC).

Feng, Q., Lixing, F., Longya, X., Ping, J., Guoliang, Z., & Jiangbo, W. (2014, 31 Aug.-3 Sept. 2014). *Si and SiC power MOSFET characterization and comparison.* Paper presented at the 2014 IEEE Conference and Expo Transportation Electrification Asia-Pacific (ITEC Asia-Pacific).

Harilal, A., Ramachandran, T., Satheesh Babu, T. G., & Suneesh, P. V. (2020). Fabrication of Silver Peroxide– Zinc Rechargeable Battery. *Materials Today: Proceedings, 24*, 949-959. doi:10.1016/j.matpr.2020.04.407

Hasan, M. R. (2017, 28-30 Sept. 2017). *Influence of device performance of Sub-10 nm GaN-based DG-MOSFETs over conventional Si-based SG-MOSFETs.* Paper presented at the 2017 4th International Conference on Advances in Electrical Engineering (ICAEE).

Hobusch, G. M., Döring, K., Brånemark, R., & Windhager, R. (2020). Advanced techniques in amputation surgery and prosthetic technology in the lower extremity. *EFORT Open Reviews, 5*(10), 724-741. doi:10.1302/2058-5241.5.190070

Hu, A. P., You, Y. W., Chen, F. B., McCormick, D., & Budgett, D. M. (2016). Wireless Power Supply for ICP Devices With Hybrid Supercapacitor and Battery Storage. *IEEE Journal of Emerging and Selected Topics in Power Electronics, 4*(1), 273-279. doi:10.1109/JESTPE.2015.2489226

Hughes, A. (2006). *Electric Motors and Drives Fundamentals, Types and Applications* (Third ed.). Burlington: Elsevier Ltd.

Hussian, J., Gelani, H. E., Ahmad, B., Ali, A., Rehman, S., & Arshad, W. (2018, 10-12 Sept. 2018). *Design and Development of EMG Controlled Prosthetics Limb with the Self-Charging Capability.* Paper presented at the 2018 International Conference on Power Generation Systems and Renewable Energy Technologies (PGSRET).

InvenSense, I. (2013). MPU-6000 and MPU-6050 Product Specification. In (3.4 ed.).

Ismayil kani, A. P. N., Manikandan, S. P. B. V., & Premkumar, A. P. K. (2021). Performance of Single Phase Soft Switching Inverter using Artificial Neural Network. *Microprocessors and Microsystems*, 104236. doi:10.1016/j.micpro.2021.104236

Jana, S., Biswas, P. K., & Das, U. (2017, 2-3 Dec. 2017). *A comparative study of two-level and five-level inverter to convert supercapacitive energy for PMSM load.* Paper presented at the 2017 IEEE Calcutta Conference (CALCON).

Jarvis, H. L., Bennett, A. N., Twiste, M., Phillip, R. D., Etherington, J., & Baker, R. (2017). Temporal Spatial and Metabolic Measures of Walking in Highly Functional Individuals With Lower Limb Amputations. *Archives of Physical Medicine and Rehabilitation, 98*(7), 1389-1399. doi:10.1016/j.apmr.2016.09.134

Koshti, A. K., & Rao, M. N. (2017, 24-26 Feb. 2017). *A brief review on multilevel inverter topologies.* Paper presented at the 2017 International Conference on Data Management, Analytics and Innovation (ICDMAI).

Kouzbary, M., Abu Osman, N. A., Kouzbary, H., Shasmin, H., & Arifin, N. (2020). Towards Universal Control System for Powered Ankle–Foot Prosthesis: A Simulation Study. *International Journal of Fuzzy Systems*. doi:10.1007/s40815-020-00855-4

Krishna, A., & Suresh, L. P. (2016, 18-19 March 2016). *A brief review on multi level inverter topologies.* Paper presented at the 2016 International Conference on Circuit, Power and Computing Technologies (ICCPCT).

Lechler, K., Frossard, B., Whelan, L., Langlois, D., Müller, R., & Kristjansson, K. (2018). Motorized Biomechatronic Upper and Lower Limb Prostheses—Clinically Relevant Outcomes. *PM&R, 10*(9S2), S207-S219. doi:10.1016/j.pmrj.2018.06.015

Lee, K., Dai, M., & Chuang, C. (2018). Temperature-Compensated Model for Lithium-Ion Polymer Batteries With Extended Kalman Filter State-of-Charge Estimation for an Implantable Charger. *IEEE Transactions on Industrial Electronics, 65*(1), 589-596. doi:10.1109/TIE.2017.2721880

Liu, J., Abu Osman, N. A., Al Kouzbary, M., Al Kouzbary, H., Abd Razak, N. A., Shasmin, H. N., & Arifin, N. (2021). Classification and Comparison of Mechanical Design of Powered Ankle–Foot Prostheses for Transtibial Amputees Developed in the 21st Century: A Systematic Review. *Journal of Medical Devices, 15*(1). doi:10.1115/1.4049437

Mahesh, K. V., Angadi, S., & Raju, A. B. (2018, 1-3 March 2018). *Single Stage PV Water Pumping System With MPPT Employing Three Phase Induction Motor.* Paper presented at the 2018 International Conference on Current Trends towards Converging Technologies (ICCTCT).

Maheswari, K. T., Bharanikumar, R., Arjun, V., Amrish, R., & Bhuvanesh, M. (2020). A comprehensive review on cascaded H-bridge multilevel inverter for medium voltage high power applications. *Materials Today: Proceedings*. doi:10.1016/j.matpr.2020.11.519

Manias, S. N. (2017). 6 - Inverters (DC–AC Converters). In S. N. Manias (Ed.), *Power Electronics and Motor Drive Systems* (pp. 271-500): Academic Press.

Patin, N. (2015). 2 - DC/AC Converters. In N. Patin (Ed.), *Power Electronics Applied to Industrial Systems and Transports, Volume 2* (pp. 35-100): Elsevier.

Qanbari, T., & Tousi, B. (2021). Single-Source Three-Phase Multilevel Inverter Assembled by Three-Phase Two-Level Inverter and Two Single-Phase Cascaded H-Bridge Inverters. *IEEE Transactions on Power Electronics, 36*(5), 5204-5212. doi:10.1109/TPEL.2020.3029870

Rodriguez, J., Jih-Sheng, L., & Fang Zheng, P. (2002). Multilevel inverters: a survey of topologies, controls, and applications. *IEEE Transactions on Industrial Electronics, 49*(4), 724-738. doi:10.1109/TIE.2002.801052

Rossi, M., Rizzi, A., Lorenzelli, L., & Brunelli, D. (2016, 30 Oct.-3 Nov. 2016). *Portable embedded systems for prosthetic interface stress mapping of lower limbs amputees.* Paper presented at the 2016 IEEE SENSORS.

Rout, P. K., Nayak, D., & Acharya, D. P. (2013, 21-23 Sept. 2013). *A novel low power 3T inverter.* Paper presented at the 2013 International Conference on Advanced Electronic Systems (ICAES).

Rowe, E., Beauchamp, M. K., & Astephen Wilson, J. (2021). Age and sex differences in normative gait patterns. *Gait & Posture, 88*, 109-115. doi:10.1016/j.gaitpost.2021.05.014

Sakunthala, S., Kiranmayi, R., & Mandadi, P. N. (2017, 1-2 Aug. 2017). *A study on industrial motor drives: Comparison and applications of PMSM and BLDC motor drives.* Paper presented at the 2017 International Conference on Energy, Communication, Data Analytics and Soft Computing (ICECDS).

Su, P. F., Gard, S. A., Lipschutz, R. D., & Kuiken, T. A. (2007). Gait characteristics of persons with bilateral transtibial amputations. *J Rehabil Res Dev, 44*(4), 491-501. doi:10.1682/jrrd.2006.10.0135

Texas Instruments. (2018). LMG5200 80-V, 10-A GaN Half-Bridge Power Stage. In (E ed.).

Thiyagarajan, V. (2020). Simulation analysis of 51-level inverter topology with reduced switch count. *Materials Today: Proceedings, 33*, 3870-3876. doi:10.1016/j.matpr.2020.06.241

Tucker, M. R., Olivier, J., Pagel, A., Bleuler, H., Bouri, M., Lambercy, O., . . . Gassert, R. (2015). Control strategies for active lower extremity prosthetics and orthotics: a review. *J Neuroeng Rehabil, 12*(1), 1. doi:10.1186/1743-0003-12-1

Tucker, M. R., Olivier, J., Pagel, A., Bleuler, H., Bouri, M., Lambercy, O., . . . Gassert, R. (2015). Control strategies for active lower extremity prosthetics and orthotics: a review. *Journal of NeuroEngineering and Rehabilitation, 12*(1), 1. doi:10.1186/1743-0003-12-1

Venkataramanaiah, J., Suresh, Y., & Panda, A. K. (2017). A review on symmetric, asymmetric, hybrid and single DC sources based multilevel inverter topologies. *Renewable and Sustainable Energy Reviews, 76*, 788-812. doi:10.1016/j.rser.2017.03.066

Vijayalakshmi, S., Hubert Tony Raj, L., Palaniyappan, S., & Rajkumar, A. (2020). A review on multilevel H-Bridge cascaded inductor less hybrid inverter for Electric vehicles with PWM control. *Materials Today: Proceedings*. doi:10.1016/j.matpr.2020.08.477

WorldData.info. Average height of men and women worldwide. Retrieved from https://www.worlddata.info/asia/malaysia/health.php

Ziegler-Graham, K., MacKenzie, E. J., Ephraim, P. L., Travison, T. G., & Brookmeyer, R. (2008). Estimating the Prevalence of Limb Loss in the United States: 2005 to 2050. *Archives of Physical Medicine and Rehabilitation, 89*(3), 422-429. doi:10.1016/j.apmr.2007.11.005